이학석사 학위논문

Elemental Variations Induced by Phosphatization and Controlling Factors of REY in Phosphatized Crusts from the Lemkein Seamount, Western Pacific

서태평양 렘케인 해산의 인산염화 작용으로 인한 망간각의 원소 변화와 희토류 원소의 조절 요인

2015 년 8 월

서울대학교 대학원

지구환경과학부

최지수

Elemental Variations Induced by Phosphatization and Controlling Factors of REY in Phosphatized Crusts from the Lemkein Seamount, Western Pacific

지도 교수 이 인 성

이 논문을 이학석사 학위논문으로 제출함
2015 년 7 월

서울대학교 대학원
지구환경과학부
최 지 수

최지수의 이학석사 학위논문을 인준함
2015 년 6 월

위 원 장 정 해 명 (인)

부위원장 이 인 성 (인)

위 원 김 종 욱 (인)

Abstarct

Elemental Variations Induced by Phosphatization and Controlling Factors of REY in Phosphatized Crusts from the Lemkein Seamount, Western Pacific

Jisu Choi

School of Earth and Environmental Sciences

The Graduate School

Seoul National University

Phosphatized crusts from the Lemkein seamount were analyzed to confirm effects of phosphatization on elemental composition. Major phases of the ferromanganese crusts were observed with their compositions using SEM and it was verified by XRD. Ten samples of specific depth in a phosphatized ferromanganese crust CD 5-5 were collected by drilling, and measured by ICP-AES for major and minor elements and ICP-MS for trace elements. Thin section faced with drilled sites were analyzed by EPMA and LA-ICP-MS. Elements such as Co, Al, Ti, Fe, As, and Mn are depleted, otherwise, other elements like Zn, Ni, and Cu are enriched compared to non-phosphatized crusts.

These major trends of elemental variation between non-phosphatized crusts and phosphatized crusts are coincident with previous study. Elemental variations are induced by recrystallization of Mn oxides, loss of Fe phases, and formation of carbonate fluorapatite (CFA). Ce enrichment is observed in discrimination diagram using REY, and Ce and Mn are strongly related based on correlation coefficients number tables (CC # tables). It suggests that Ce is enriched in one of Mn oxide phases rather than CFA. Positive correlation between REE and Ca/P ratios with increasing correlation coefficients as increasing atomic number is observed. It indicates that REE contents are controlled by anion composition of CFA at similar P concentrations in phosphatized crusts. Y also displays analogous correlations, but is less remarkable than REE. LA-ICP-MS displays distinct differences between the phases composing phosphatized crusts, and respective phases have typical REY pattern depending on major phases of ablated area. Total REE contents except Ce are enriched in CFA aggregates and are depleted in todorokite. REY contents and patterns are controlled by loss of primary ferromanganese phases and compensation by secondary phosphatized phases.

Keywords : Ferromanganese crust, rare earth elements and Yttrium (REY), phosphatization, carbonate fluorapatite (CFA), Ca/P ratio

Table of Contents

List of tables

List of figures

1. Introduction

Ferromanganese crusts are recognized future resources with ferromanganese nodules. Variable elements, such as Co, Ti, Mn, Ni, Pt, Zr, Nb, Te, Bi, Mo, W, Th, and rare earth elements (REEs), are enriched in crusts (Hein et al., 2013; Hein and Koschinsky, 2014). Formation mechanism and environmental study of metals in ferromanganese crusts are widely studied but not solved clearly (Halbach, 1986; Koschinsky and Halbach, 1995; Wen et al., 1997; Koschinsky et al., 2003; Wang and Muller, 2009; Wang et al., 2009; Wang et al., 2011; Hein et al., 2012; Loges et al., 2012; Little et al., 2014; Schmidt et al., 2014). Ferromanganese crusts are not only important as resources but also as paleoceanographic records, since composition of crusts is controlled by regional and global oceanic conditions (Wen et al., 1997; Frank et al., 1999; Koschinsky et al., 1996; Hein and Koschinsky, 2013). Isotope study of ferromangane crusts are the other important field of the study (Godfrey et al., 1997; Ling et al., 1997; Frank et al., 1999; Klemm et al., 2005; Horner et al., 2010). However, problematic layer is included in ferromanganese crusts. The layer is phosphatized crusts, and it does not used in paleoceanographic study, nor follows general enrichment trend of

ferromanganese crusts (Bau et al., 1996; Koschinsky et al., 1997).

Phosphatization is most important secondary process of ferromanganese crusts. Expansion of the suboxic oxygen minimum zone (OMZ) following increased productivity of surface waters promotes the precipitation of phosphorite at the phosphate-rich water. Ferromanganese crusts are impregnated by phosphorite, mainly form of carbonate fluorapatite (CFA). Phosphatized crusts appear at the old layer of ferromanganese crusts because of episodes of phosphatization: late Eocene to early Miocene (21-39 Ma) on mid-Pacific seamounts discontinuously (Halbach and Puteanus, 1984; Halbach et al., 1989; Hein et al., 1993; Koschinsky et al., 1997; Glasby et al., 2007; Hyeong et al., 2013). Phosphatization affects variable features of ferromanganese crusts. Crystallography of ferromanganese crusts is changed by phosphatization from Fe-bearing vernadite and X-ray amorphous iron oxyhydroxide to todorokite, goethite, both usually constitute diagenetic ferromanganese nodules, and CFA. As a result of recrystallization to more stable phase, remobilization of elements which are composing former phase is occurred. It is revealed that some elements such as Si, Fe, Al, Ti, Co, Mn, and Pb are depleted, and others like Ni, Zn, Cu, Y, and REEs are enriched in phosphatized crust

compared to non-phosphatized crusts mostly (Puteanus and Halbach, 1988; Koschinsky et al., 1997). However, different observation of elemental redistribution on a small scale analysis is reported. Depleted elements are Co, Ni, Mg, Al, Mn, Si, Cu, Zn, and Fe, and enriched elements are P, Ca, Ba, Pb, Sr, and REEs (Pan et al., 2005). These kinds of study usually use correlation to observe group of related elements in ferromanganese crusts (De Carlo and McMurtry, 1992; Koschinsky and Halbach, 1995; Wen et al., 1997; Hein and Morgan, 1999; Hein et al., 2003), but phosphatized crusts were included with non-phoshatized crusts (Wen et al, 1997; Pan et al., 2005) or were not included in analyzed sets (Hein and Morgan, 1999). Sequential leaching is used for distribution of elements between the major phases of ferromanganese crusts (Koschinsky and Halbach, 1995; Kuhn et al., 2003; Koschinsky and Hein, 2003; Takahashi et al, 2007, Bau and Koschinsky, 2009). However, sequential leaching of phosphatized crusts has problem. It is that CFA is soluble in other phases besides major leaching phase, and Mn oxide phases are not distinguished separately (Koschinsky and Hein, 2003). Elemental effects of phosphatization to ferromanganese crusts are yet unclear in some part such as Ni and REY (Hein et al., 1988; Bau et al., 1996; Koschinsky et

al., 1997). Ni can be incorporated into todorokite (Bodei et al., 2007; Peacock and Sherman, 2007), and Ni-rich ferromanganese crust is also observed in non-diagenetic signal ferromanganese crusts from the Shatsky Rise (Hein et al., 2012). REY except Ce is thought to be substitute Ca^{2+} of CFA (McLlellan, 1980; McArthur and Walsh, 1984; Koschinsky et al., 1997; Piper and Perkins, 2014). Bau et al. (1996) assumed REY-bearing phase except CFA to explain observed Y/Ho ratio and P contents. Ce is scavenged by oxidation on surface of Mn oxide and Fe oxyhydroxide. This process represents redox condition of ferromanganese crusts precipitation. Ce is mainly adsorbed in Mn oxide, and also adsorbed in Fe oxyhydroxide (Otha and Kawabe, 2001; Bau and Koschinsky, 2009). However, scavenging of Ce is also kinetic process, so it is affected by rate of precipitation (Kuhn et al., 1998; Takahashi et al., 2007). Positive Ce anomaly is also observed in phosphatized crusts, and it is related with redox condition (Bau et al., 1996; Koschinsky et al., 1997). LA-ICP-MS was used for study of ferromanganese crust, it is challenging method, yet (Garbe-Schonberg and McMurtry, 1994; Axelsson et al., 2002; Barefoot, 2004).

This study aims to know more elaborate relations between elements of phosphatized crusts and elemental effects of

phosphatization especially for REY. LA-ICP-MS is conducted to see REY contents of several phases in phosphatized crusts. There are some suggestions about biogenic formation of ferromanganese crusts (Wang and Muller, 2009a and b; Wang et al., 2009; Wang et al., 2011) and diatom diagenesis (Jeong et al., 2000). They are not considered in this study.

2. Samples

Two hydrogenetic Fe-Mn crusts (Lemkein 99-1 CD 1-5 and Lemkein 99-1 CD 5-5) were chosen for this study. CD1-5 was recovered at about 2700m water depth in the central western Pacific (9° 19' N, 166° 08' E; KODOS, cruise Onnuri), CD 5-5 was dredged at about 2200m water depth in the central western Pacific (9° 28' N, 166° 05' E; KODOS, cruise Onnuri) both the crusts from the Lemkein seamount. (Fig. 1 and Table 1)

CD1-5 has two non-phosphatized layers and does not contain substrate rock. CD 5-5 has a phosphatized layer and two non-phosphatized layers, and it is encountered with substrate rock, which is phosphatized carbonate. The phosphatized layer of CD 5-5 is interpenetrated by CFA. Both of the non-phosphatized layers have same textures. The upper most layers are darker, denser and thin crust, and second layers of non-phosphatized crust are porous with reddish particles. Third layer of CD 5-5 is phosphatized crust. Non-phosphatized first layers of CD 1-5 and CD 5-5, phosphatized layer of CD 5-5 are used in this study to determine effects of phosphatization to elemental redistribution of ferromanganese crusts. (Fig. 2)

3. Methods

Phosphatized layer of CD 5-5 and non-phosphatized layer of CD 1-5 were extensively observed with scanning electron microscope (SEM) both back-scatter and secondary electron images and energy dispersive X-ray spectroscopy (EDS) using JEOL JSM-6610 at Korea Polar Research Institute (KOPRI).

Sampling for quantitative analysis and X-ray diffraction (XRD) of phosphatized crust and substrate rock of CD 5-5 and non-phosphatized crust of CD 1-5 were done using dental drill. One substrate rock sample, ten phosphatized crust samples and one non-phosphatized crust sample of CD 5-5 and one non-phosphatized sample of CD 1-5 were collected. Visible phosphorite was removed by hand picking. Sampling sites on crusts were connivent at the upper-most crusts of non-phosphatized layer and lower 20mm depth crusts from the boundary between substrate rock and ferromanganese crusts of phosphatized layer as marked at Fig. 2. The upper-most crusts were selected for representative sample of non-phosphatized crusts that are formed at the present. Sampling of phosphatized crusts was designed for minimizing effects of the environments on which

ferromanganese crusts were formed. Depth of sampling sites was also planned for reducing variation of dilution effects by carbonate fluorapatite (CFA). Phosphorous concentrations of sampled depth of crusts were nearly constant as 3.36 to 4.17 (average 3.87 wt %). XRD were made using Miniflex 600 at G2MAT laboratory, SNU. X-ray setting was 40kV and 15mA with scan speed 1.5 deg/min. Drilled samples were dried at 105℃ for 24 h to adjust 0% hygroscopic condition. Mg, Al, P, K, Ca, Ti, V, Mn, Fe, Co, Ni, Cu, Zn, As, Sr, Ba, and Pb were analyzed by Optima 4300 DV Inductively Coupled Plasma Atomic Emission Spectroscopy (ICP-AES). REYs, Cd, Pt, Tl, Th, and U were determined by Elan 6100 Inductively Coupled Plasma Mass Spectrometer (ICP-MS). Digestion and quantitative analysis was conducted at National Center for Inter-University Research Facilities (NCIRF), SNU. Correlation analysis of quantitative analysis was performed on Microsoft Excel. Non phosphatized crusts CD 1-5 and CD 5-5 are mainly treated as comparison group to phosphatized crusts. JEOL JXA-8230 Electron probe microanalyzer (EPMA) at KOPRI and Laser Ablation Inductively Coupled Plasma Mass Spectrometer (LA-ICP-MS) at Korea Basic Science Institute (KBSI) were used for measurement of REY in phases of phosphatized crusts, respectively.

EPMA measurement aimed to get two kinds of data; Point quantitative analysis of major and minor elements such as Na, Mg, Al, Si, P, S, K, Ca, Mn, Fe, Ni, and Ce in phosphatized crusts and major element data for standardization of LA-ICP-MS. Voltage is 15kV and probe diameter is 5 μm for the first data. 15kV and defocused beam with 50 μm probe diameter was set for second data. LA-ICP-MS was conducted for comparing REY contents of phases in phosphatized crusts. Laser ablation system was New Wave UP-213, ICP-MS was Thermo X2. RF power was 1300W, Ar nebulizer flow was 0.73L/min, Ar auxiliary gas was 0.85L/min, Ar cooling gas was 13.5L/min, laser wavelength was 213nm, He carrier gas was 0.7L/min, repetition rate was 10Hz, energy density was 10J/cm^3, dwell time was 10ms, and beam size is 55 μm. 29Si, 43Ca, 44Ca, 56Fe, 58Fe, 65Cu, 89Y, 139La, 140Ce, 141Pr, 146Nd, 147Sm, 153Eu, 157Gd, 159Tb, 163Dy, 165Ho, 166Er, 169Tm, 172Yb, and 175Lu was analyzed. Data was calculated by program Glitter.

4. Results

4.1 SEM

SEM is conducted to observe textures, micro structures, mineral distribution with major elements ratios of ferromanganese crusts from the Lemkein seamount. Non-phosphatized crusts and phosphatized crusts have various differences in elemental compositions and textures.

4.1.1 Non-phosphatized crust CD 1-5

CD 1-5 has two distinct textures. Columnar with laminated and massive texture is mainly composed of Mn oxide which is thought Fe-bearing vernadite (Fig. 3-a and b). Another texture is columnar and botryoidal with mottled Fe-rich part thought Fe oxyhydroxide (Fig. 3-c and d). Fe has more fraction than Mn in mottled Fe-rich part. Mn-rich part is whiter than Fe-rich part. Occurrence of Fe mottled texture does not have any regular rule such as layer divided by depth. Major elements of non-phosphatized crusts such as Mn, Fe, Si, and Ca are measured with EDS. Range of Mn/Fe ratio on Fe-bearing vernadite is totally 1.1 to 5.1. It is, however, separated by texture as 1.9 to 5.1 at columnar texture and 1.1 to 2.6 at mottled texture. Mn/Fe ratio on Fe oxyhydroxide is not divided by texture and has range 0 to 1.5. Si and

Ca concentrations have correlation with Mn/Fe ratio (Table 2). Positive correlation between Si and Mn/Fe ratio indicates Si is associated with Fe oxyhydroxide. It is coincident with formation mechanism of ferromanganese crusts that silicate and iron hydroxide form mixed colloids (Koschinsky and Halbach, 1995) and statistical associations of Fe and Si as detrital groups (Wen et al., 1997). Otherwise, Ca and Mn/Fe ratio have negative correlation. It means that Ca fraction is more closed to Mn fraction than Fe fraction in non-phosphatized crusts.

4.1.2 Phosphatized crust CD 5-5

Phosphatized crust CD 5-5 has monotonous texture entirely. Micro CFA fills Fe-bearing vernadite imprinting wave pattern (Fig. 5-b, c, and f). However, complicate structures occur near bulky phosphorite infillings (Fig. 4-a, c, and d, Fig. 5-a, d, and e). Fig. 4-a is phosphorite with biogenic mold and ferromanganese crusts formation. Mn and Fe fraction of ferromanganese crusts in phosphorite have distinct separation. Some growth columns of crusts are composed of Mn oxide and CFA, but the others consist of Fe oxyhydroxide and CFA mainly. 4-b is boundary between phosphatized carbonate substrate

rock and ferromanganese crust. It is general that boundary is clear between substrate rock and ferromanganese crust, but substrate rock and ferromanganese crust are partly mixed in phosphatized substrate rock. Fig. 4-c shows overall mineralogy of phosphatized crusts. EDS data of Fig. 4c are classified three phase; Considerable concentration of Mn and Fe with Mn/Fe ratio 1.2 to 1.5, extremely high Mn and Mn/Fe ratio with 5 wt% Ni, and CFA having Ca and P as major component (Table 3). Former two phases are thought to be Fe-bearing vernadite with CFA infillings and todorokite. Fig. 4d is CFA envelopment of Fe-bearing vernadite with CFA grains. White rims and aggregates are todorokite based on 30 to 60 wt% Mn with high Mn/Fe ratio and 3 to 6 wt% Ni. Todorokite is distributed closed to the structure such as bulky phosphorite infillings (Table 3, Fig. 5a, d, and e). Fe-bearing vernadite with 1.3 to 3.7 Mn/Fe ratios is general phase in phosphatized crusts. CFA usually associated with vernadite and also occurs as micro vein (Table 3 and Fig. 5a). Ti-rich grain is observed and occurs similarly such as micro-filling CFA. It seems to be occurred in phosphatized crusts infrequently and has brighter contrast than CFA.

4.2 XRD

XRD data of ferromanganese crusts had low intensity and wide width to distinguish mineral phase obscurely. Mineral matching with XRD data is performed by comparing major peaks of the data and major peaks information of representative minerals known as component of each part of ferromanganese crusts.

Major peaks of non-phosphatized crust of CD 1-5 are 5.59, 36.53, and 65.87. First major peak is thought artifact came from low angle setting. Other peaks are matched with vernadite and iron oxyhydroxide peaks. (Fig. 6)

Phosphatized crust of CD 5-5 has more major peaks than non-phosphatized layer of CD 1-5. Major peaks other than overlapped range with non-phosphatized layer are associated with fluorapatite. Artifact observed near zero degree does not apper at phosphatized layer of CD 5-5. Fluorapatite, vernadite, todorokite, and goethite are composing phosphatized layer of CD 505 based on XRD data. (Fig. 7)

XRD data of CD 5-5 substrate rock are more complex than the crusts data. Fluorapatite, calcite, quartz, goethite, zeolite, and labradorite are matched with peaks of CD 5-5 substrate rock XRD data.

Other minerals such as aluminosilicate mineral and calcium silicate mineral also have similar peak with observed XRD data of CD 5-5 substrate rock. (Fig. 8)

4.3 Quantitative analysis

Three groups of ferromanganese crusts are measured; Two non-phosphatized crust of CD 1-5, a non-phosphatized crust of CD 5-5, and ten phosphatized crusts of CD 5-5. Ten phosphatized crusts of CD 5-5 are focused on relationship between elements and effects of phosphatization. To do this, different sampling method is used as mentioned above. This method is designed for minimizing effect of environmental compositional variation and intensity of phosphatization based on phosphorous concentration. Three non-phosphatized crusts samples are analyzed for comparison groups. However, CD 1-5 has significant difference of chemical composition such as K, REYs, Mn/Fe ratio and Ca/P ratio with CD 5-5 thought to be induced by different formation depth (Table 4 and Table 5). For this reason, only non-phosphatized crust of CD 5-5 is used as representative of ferromanganese crusts that is not affected by phosphatization at the

Lemkein seamount in discussion of this study.

4.3.1 Comparison between non-phosphatized crust and phosphatized crust CD 5-5

Major, minor, and trace elemental compositions of ferromanganese crust CD 5-5 samples are on list (Table 5). Relative percentage of phosphatized crusts to non-phosphatized crusts is calculated (Fig. 9). 0% means phosphatized crusts have same amount of elements with non-phosphatized crusts. Positive percentage is enrichment of elements in phosphatized crusts compared to non-phosphatized crusts. Otherwise, negative percentage indicates depletion of elements in phosphatized crusts compared to non-phosphatized crusts. In major and minor elements, P, Ca, Ni, Ba, and Sr are enriched. However, Mn, Mg, Pb, K, Fe, Ti, Al, and Co are depleted elements in phosphatized crusts. Enrichment of Ce, Th, and Cu and depletion of Y, Cd, V, Pt, Tl, REE, U, and As are displayed among trace elements variations. P and Ca are enriched 830% and 357% each compared to non-phosphatized crusts resulting from formation of CFA. Formation of CFA causes dilution effects in ferromanganese crusts with compensation of elements such as Ba, Sr, Y, and REEs that can be

incorporated in stable phosphatic compounds (Nathan, 1984; Koschinsky el al., 1997). Mn, Mg, K, Ni, Cu, and Zn are associated with recrystallization of Fe-bearing vernadite to todorokite. Fe and its relevant elements such as Ti, Al, and As show negative variations due to loss of Fe phase in non-phosphatized crusts (Koschinsky et al., 1997).

Mn/Fe, Ca/P, and Y/Ho ratios between non-phosphatized crusts and phosphatized crusts also are distinguishable factor. Phosphatized crusts have higher Mn/Fe ratio with 2.81 to 4.62 due to loss of Fe phase during phosphatization. Low Ca/P ratio with 2.49 to 3.26 and high Y/Ho ratio with 18.30 to 45.30 come from formation of CFA mainly. Ca/P ratios of some phosphorites are 2.65 for francolite, 2.16 for fluorapatite, and 2.63 for equatorial Pacific phosphorite (Hein et al., 1993). Y/Ho ratio is 18.5 to 44.9 that is similar or slightly high value compared to non-phosphatized crusts (Bau et al., 1996).

Th is characteristic element of open-ocean Pacific crusts as its low concentration (Hein et al., 2012). It is reported that substrate rock does not affect composition of its overlying ferromanganese crusts and phosphatized substrate rock seems to affect its overlying

ferromanganese crusts due to phosphatization of ferromanganese crusts (Hein and Morgan, 1999). However, Th concentrations of boundary samples C0, C1, L1, and R1 have higher concentrations than other samples. Other elements correlated with Th such as Al, Ti, Fe, and Sr also have similar trend, but their variations are not clear like Th. It is interesting, but not a scope of this study.

4.3.2 Correlation coefficients of analysis - CC # tables

Correlation coefficients of ten bulk analyses of phosphatized crust CD 5-5 from the Lemkein seamount are listed (Table 6). REY and major elements such as Mn, Fe, P, and Ca with Ca/P ratio and Mn/Fe ratio are calculated separately (Table 7). Correlation coefficients tables are hard to identify relationship between elements intuitively due to a lot of analyzed elements, so CC # tables are used in this study (Table 8). It is simplified form of correlation coefficients table, and present only positive or negative mark of correlation between major phase elements such as Mn, Fe, Ca, and P with their ratio and analyzed elements. # of CC # is criterion of marked correlation. CC 90 show positive or negative correlations that have correlation coefficients above 0.90. Thus CC # tables are easy to know correlation between

phases and elements as changing correlation coefficients. Elements that have similar trend are arranged together from major and minor elements to trace elements. Crust phase are composed of Mn, Fe and Mn/Fe ratio fraction in CC # table. Mn fraction represents all Mn oxide phases including Fe-bearing vernadite and todorokite. Fe fraction indicates iron in Fe-bearing vernadite and minor fraction of goethite. Mn/Fe ratio can be interpreted in two ways. Phosphatized crusts were undergone loss of Fe, dilution effects by formation of CFA and recrystallization of Fe-bearing vernadite to todorokite during phosphatization. Mn/Fe ratio is increased as a result of phosphatization, and its value indicates amount of iron loss and recrystallized todorokite. CFA phase is composed of Ca and P fraction with Ca/P ratio. Both Ca and P fraction are increased by formation of CFA during phosphatization, but Ca is precipitated from seawater or come from calcite and P is originated from seawater largely. Ca of CFA phase can be substituted by some elements including Sc, Sr, Y and REE. P of CFA phase forms phosphate PO_4^{3-} and it can also be substituted by other anions such as CO_3^{2-} and SO_4^{2-} (Gulbrandsen, 1966; Nathan, 1984; McClellan, 1980; Piper and Perkins, 2014). Ca/P ratio is complex factor including all of substitutions in CFA, and other fractions of CFA

phase indicate effect of CFA formation but also contain their substitution. Fe is only element that has mark on cc # table among major elements. Mn participates in recrystallization. Its loss during phosphatization is lower than Fe, so Mn/Fe ratio is more dependent on Fe. Minus mark between Fe and P on CC 60 is due to variation difference between Ca and P. This also indicates dilution effects of CFA are more dependent on P than Ca. First factor of variation of K, Ni, and Zn is formation of todorokite based on Mn/Fe ratio and next is lower Fe contents. Ti, Al, Sr, Pb, U, and Th are related with loss of Fe phase during phosphatization based on positive mark of Fe fraction and negative mark of Mn/Fe ratio. Cu is also known as incorporated in todorokite, but major phase containing Cu is Fe fraction both non-phosphatized crust and phosphatized crust (Koschinsky and Hein, 2003). Thus, Cu has mark same with Fe associated elements though it is enriched in phosphatized crusts resulted from its incorporation into todorokite. Ce is marked positively with Mn fraction on CC 90, and this indicates its enrichment on Mn fraction during phosphatization. V and As are controversial and not solved clearly. CFA phase mainly have negative marks that represent loss of Fe fraction. REE and Y, however, have positive mark, and this indicates they are incorporated in CFA

compensating primary REY loss due to losing of original Fe and Mn fraction of ferromanganese crusts having high REY contents. Elements that do not have mark on CC # such as Ba are associated with more than one phase or they are not associated with mentioned phase above. Trend of correlation coefficients and elemental variations differ with previous study (Wen et al., 1997; Koschinsky et al., 1997; Pan et al., 2005), but these differences are come from sampling methods. Previous study collected samples bulk layer or specific depths, but in this study, samples were selected only in lower parts of phosphatized crust not whole phosphatized crusts as mentioned above.

4.4 EPMA

3μm and 5μm beam for quantitative analysis and defocused 50μm beam for LA-ICP-MS were used to EPMA. Todorokite, vernadite, and CFA were analyzed to 3μm and 5μm beam respectively (Table 9). Differences between todorokite and vernadite were appeared. Al_2O_3, MnO_2, MgO, and NiO were enriched in todorokite. Otherwise, Fe_2O_3, CaO, and Na_2O were enriched in vernadite. Recrystallized todorokite in phosphatized crusts are distinguished with todorokite in

ferromanganese nodules (Banerjee et al., 1999). Todorokite in ferromanganese crusts has higher Ni, Al, and Fe contents. Vernadite in phosphatized crusts has higher Mn contents compared to primary todorokite in ferromanganese nodules. Those differences indicate Mn phases are concentrated during phosphatization accompanied by loss of Fe phases. Ce was included in analyzed elements because it is known that ferromanganese crusts have higher Ce contents and Ce contents are above detection limit. Two kinds of CFA are found in phosphatized crusts, and they have significant difference of their chemical composition including Ce contents (Fig. 13a). Their differences are suspected to come from different formation mechanisms followed by anion compositions. Defocused beam was conducted for using major element data on LA-ICP-MS (Table 10).

4.5 LA-ICP-MS

It is hard to analyze CFA and Fe-bearing vernadite respectively in phosphatized crusts because size of CFA is about 1 μm infilling Fe-bearing vernadite. LA-ICP-MS was planned to compare todorokite major spots, Fe-bearing major spots, and CFA major spots. EPMA was

conducted before LA-ICP-MS for known concentration method using CaO EPMA data (Table 10). Traces were remaining after EPMA, and LA-ICP-MS was set to ablate the trace (Fig. 13b). Data reduction was done on former few seconds from the time when ferromanganese spectra were occurred to the time on which different spectra pattern was appeared. General reduction method is using intermediate spectra of samples. However, phosphatized ferromanganese crust is thought that using former spectra is proper method due to its highly heterogeneous characteristic. LA-ICP-MS data in this study are representative of surface composition, hence the reason of data reduction methods (Table 11).

Total REE contents except Ce, Y/Ho ratio, and $Ce_{SN}/Ce_{SN}*$ are distinctive between the phases such as todorokite, vernadite, and CFA. Vernadite phases are divided to three different vernadite. Ver-1 contains fibrous todorokite. Ver-2 is located at same depth with ver-1, but do not contain fibrous todorokite. Ver-2 has most abundant CFA fraction among vernadite phases. Ver-3 is located the lower most part of phosphatized crusts and near the CFA aggregates. CFA aggregates have the highest total REE contents, otherwise, todorokite have the lowest total REE contents. High Y/Ho ratio is requirement for

explanation of mixing results and P contents in phosphatized crust (Bau et al., 1996). However, High Y/Ho ratio above 44 which is the highest Y/Ho ratio in phosphatized crust in Bau et al. (1996) is only present at ferromanganese crust inside CFA envelope (Fig. 4d). Shale normalized REY patterns also show distinct differences between the phases in phosphatized crusts (Fig. 14). Todorokite have typical REY pattern of non-phosphatized crust and vernadite display archetypal REY pattern of phosphatized crust except vernadite in CFA envelope that has higher Y/Ho ratio than other phases. Ce anomaly is calculated by Ce_{SN}/Ce_{SN}^*.

$$Ce_{SN}/Ce_{SN}^* = Ce_{SN}/(0.5*La_{SN} + 0.5*Pr_{SN})$$

Ce anomaly decreases in the order of ver1, todorokite, CFA aggregate, ver3, and ver2. Vernadite in CFA envelope has lowest Ce anomaly. Those distinctions between the phosphatized phases indicate elemental migration during phosphatization.

Some problems existed on LA-ICP-MS of ferromanganese crusts. They are standard of ferromanganese samples, comparison method, and analyzation settings. Those are due to heterogeneous characteristic of ferrogmangnese crusts largely.

5. Discussions

5.1 Classification of ferromanganese crusts from the Lemkein seamount

Marine ferromanganese deposits are traditionally distinguished using the ternary Mn−Fe−10(Ni+Co+Cu) discrimination diagram (Bonatti et al. 1972). However, this discrimination diagram is hard to distinguish some of hydrothermal deposits and diagenetic deposits. A new discrimination tool is proposed based on REY distribution (Bau et al., 2014). Phosphatized crusts are not plotted usually on discrimination diagram, so phosphatized crusts are plotted using both the methods in this study (Fig. 10 and Fig. 11). Phosphatized crusts from the Lemkein seamount are plotted middle of hydrogenetic and diagenetic area on Mn−Fe−10(Ni+Co+Cu) tertiary diagram. It is ambiguous because some crusts are also plotted outside of hydrogenetic area (Fig. 10; Hein et al., 2012). REY discrimination is also uncertain to distinguish phosphatized crusts with non−phosphatized crusts similar with the tertiary diagram (Fig. 11−b). However, it displays that higher Ce_{SN}/ Ce_{SN}* and Y_{SN}/Ho_{SN} ratios of phosphatized crusts than hydrogenetic ferromanganese crusts and

nodules. REY discrimination is better method for discrimination of phosphatized crusts using Ce_{SN}/ Ce_{SN}* and Y_{SN}/Ho_{SN} ratios (Fig. 11-a). It is identified through REY discrimination that phosphatized crusts have higher Y_{SN}/Ho_{SN} ratios than hydrogenetic crusts and nodules induced by formation of CFA and Ce is enriched in phosphatized crusts. Ce enrichment in phosphatized crusts is discussed next section.

5.2 REY in phosphatized crust CD 5-5

REY in phosphatized crusts are composed of primary REY and secondary REY. Primary REY is released from ferromanganese crusts during phosphatization, and it arise from dissolution of Fe and Mn fraction. Formation of CFA and recrystallized Mn and Fe fraction compensate loss of REY. REY except Ce are mainly associated with CFA and Ce is strongly related to Mn fraction in phosphatized crust based on correlation coefficients of this study and conclusions of previous studies. However, calculation of secondary REY used by Koschinsky et al. (1997) is not a good method to consider REY changes in phosphatized crusts because of negative value of secondary REY. For CD 5-5, for example, secondary Y calculated by Koschinsky

et al. (1997) is −0.65 ppm averagely. This is because of simple reason that phosphatized crusts can have lower REY contents than non-phosphatized crusts. It is also hard say that phosphatized crusts are enriched in REY compared to non-phosphatized crusts. It should be modified for using generally in phosphatized crusts. However, it can be said that REY was largely affected by phosphatization based on Y/Ho ratio and Ce anomaly.

5.2.1 Ce enrichment in phosphatized crust CD 5-5

Ce is reserved in surface of Mn oxide and Fe oxyhydroxide as oxidative scavenging. Ce^{4+} is less soluble than Ce^{3+} and other REEs, so it do not released to seawater after adsorbed on the surface with oxidation (Bau and Koschinsky, 2009). Positive anomaly of Ce is usually observed in hydrogenetic ferromanganese crusts and nodules. This process is thought be related with redox condition of ferromanganese precipitation, so it is used as paleoceanographic study. However, the amount of anomaly is connected with kinetic process rather than redox process similar with Co.

Enrichment of Ce in phosphatized crusts can elicit two possibilities based on strong positive anomaly (Fig. 12), correlation

between Mn and Ce (Table 6), and prevalent mechanism of phosphatization. It is existence of highly Ce enriched Mn oxide phases and possibility of oxidative scavenging in reducing environments. Todorokite and vernadite is Ce enriched Mn oxide phases based on LA-ICP-MS data. It is observed that phosphorites that formed with micro-nodules have negative Ce anomaly because of preferential scavenging of Ce to micro-nodules (Dubinin et al., 2013). Thus, CFA in ferromanganese crusts also can have negative anomaly. Negative Ce anomaly is appeared at vernadite in CFA enveloped. It indicates that spheric structure has low Ce affinity during phosphatization than the other prevail phases such as todorokite and the other vernadite encountered with the structure. Excluding scavenging of Ce to Mn oxides, CFA would have Ce concentration as Ce* that is calculated through La and Pr rather than have positive Ce anomaly. The problem is whether and how Ce is incorporated in Mn oxide phases. Oxidative scavenging of Ce is kinetic process. If it is occurred during phosphatization of ferromanganese crusts, other elements attributed its contents to surface oxidation such as Co and Tl (Murray and Dillard, 1979; Bidoglio et al., 1993) are also considered. However, Co and Tl are depleted in phosphatized crusts compared to non-phosphatized

crusts. Co has same correlation trend with Ce, otherwise, Tl does not have correlation with Mn and other major elements. Enrichment mechanism during phosphatization is not clear and it was reported that REY pattern of oxic and anoxic seawater that anoxic seawater has Ce positive anomaly (Bau et al., 1997). Nonetheless, Ce enrichment in any Mn phase is necessary for explaining Ce contents in phosphatized crusts.

5.2.2 Ca/P ratio and REY correlation coefficients of phosphatized crust CD 5-5

REY is incorporated to CFA during phosphatization and its contents are variable in phosphatized crusts. It is hard to say phosphatized crusts are enriched in REY compared to non-phosphatized crusts. Enrichment of REY in phosphatized crusts is problem of REY compensation of secondary phases such as CFA, Fe-bearing vernadite, and todorokite. REE has considerable correlation coefficients with Ca/P and Ca, but negative correlation with P. This indicates concentration of REE in phosphatized crust is controlled by composition of CFA, especially, anions of CFA such as carbonate and sulfate. It could means just mixing ratio, but in natural phosphorites

have Ca/P ratios 2.57 to 2.91 (Hein et al., 1993). In this study, Ca/P ratios of phosphatized crust are 2.49 to 3.26 (Table 5). REE in phosphorites is enriched as increasing latitude (Hein et al., 1993), but in this study all samples have same latitude. It is observed that correlations of REE are increased as atomic number increases. It is coincident with stability of REE complex with carbonates. Sulfate substitution accompanies REE substitution is suggested, however it includes substitution of Na. some of SEM-EDS data targeted in CFA have Na contents about 1 wt%. Marine CFA have high sulfate contents than other CFA is also observed. Any other phases except CFA in phosphatized crusts such as REY phosphates were suggested (Bau et al., 1996), it can affects Ca/P ratios in phosphatized crusts. Two kinds of CFA were found during EPMA. One had higher Ce contents and Ca/P ratio and the other had lower Ce content and Ca/P ratio. This should be studied more. Y also display similar correlations, but less remarkable than REE.

5.2.3 REY patterns of ferromanganese crusts from the Lemkein seamount

REY patterns of ferromanganese crusts from the Lemkein

seamount are general, but slightly HREE is enriched than MREE (Fig. 12) like ferromanganese crusts of central pacific (Bau et al., 1996). It is also similar with seawater REE pattern that HREE is enriched than LREE except Ce (Byrne and Kim, 1990). REE can be variable between water depths (De Carlo and McMurtry, 1992; Zhang and Nozaki, 1996). Mn oxide preferentially scavenges HREE, but Fe oxide has preference of LREE sorbtion (Aplin, 1984; Hein et al., 1988). However, recent studies do not suggest previous observations (Otha and Kawabe, 2001; Bau and Koschinsky, 2009). Difference between non-phosphaitzed crust and phosphatized crust CD 5-5 is amount of normalized value and anomalies. Contents of REE except Ce are enriched in non-phosphatized CD 5-5, otherwise Ce in enriched in phosphatized crust CD 5-5. Gd anomaly is moderated in phosphatized crust, and Y anomaly is diametrical. This is mainly due to loss of Fe phase and formation of phases that have positive Y anomaly because Fe phase has large amount of REY proportion in phosphatized crusts that show negative Y anomaly (Bau, 1999; Bau and Koschinsky, 2009). Phosphatized crust have positive Y anomaly, and reason of change of Y anomaly is formation of CFA with incorporation of Y into CFA. REY patterns of phosphorite except Ce anomaly are similar with seawater

REY pattern (Hein et al., 1993). Secondary REY has seawater REY pattern, and it indicates that REY of phosphatized crusts are mainly secondary REY except Ce (Bau et al., 1996; Koschinsky et al., 1997; Bau et al., 2014). It is also have some influence to REY pattern of phosphatiazed crusts that REE sorption preference between Mn and Fe oxide phase mentioned above. REY pattern of LA-ICP-MS data also have typical shape as their major phases. Bulk REY is affected by respective phases composing that bulk part of crusts.

6. Conclusions

Phosphatized crusts from the Lemkein seamount are studied with new sampling way. Samples were drilled specific depth of phosphatized crusts that have similar phosphorous contents about 3 to 4 wt % Samples were collected in specific depth of sample CD 5-5. Chemical composition of the samples are similar with previous study such as depletion of Co, Al, Ti, Fe, As, and Mn and enrichment of Zn, Ni, and Cu compared to non-phosphatized crusts. Well-known tendency of these elements variatioin is explained by recrystallization of Fe-bearing vernadite to todorokite and formation of CFA during phosphatization. Classification of phosphatized crust using REY distribution displays that Ce is enriched in phosphatized crusts. Trend of correlation coefficients are analogous with previous study, but there are some difference and new observations. Enriched Ce is strongly related with Mn phases in phosphatized crusts, and REE is more connected with Ca/P ratio than Ca and P itself. This can indicate that REY contents are controlled by composition of anion of CFA such as phosphate, sulfate, and carbonate with increasing REY contents as decreasing ratio of P. REY contents and patterns are controlled by loss of primary ferromanganese phases and compensation by secondary

phosphatized ferromanganese phases. LA-ICP-MS displays distinct differences between the phases composing phosphatized crusts, and respective phases have typical REY pattern depending on major phases of ablated area. Total REE contents except Ce are enriched in CFA aggregates and are depleted in todorokite.

References

Axelsson, M.D., Rodushkin, I., Baxter, D.C., Ingri, J., Ohlander, B., 2002. High spatial resolution analysis of ferromanganese concretions by LA-ICP-MS. Geochem Trans 3, 40-47.

Banerjee, R., 1999. Petrogenesis of ferromanganese nodules from east of the Chagos Archipelago, Central Indian Basin, Indian Ocean. Mar Geol 157, 145-158.

Barefoot, R.R., 2004. Determination of platinum group elements and gold in geological materials: a review of recent magnetic sector and laser ablation applications. Anal Chim Acta 509, 119-125.

Bau, M., 1999. Scavenging of dissolved yttrium and rare earths by precipitating iron oxyhydroxide: Experimental evidence for Ce oxidation, Y-Ho fractionation, and lanthanide tetrad effect. Geochim Cosmochim Ac 63, 67-77.

Bau, M., Koschinsky, A., 2006. Hafnium and neodymium isotopes in seawater and in ferromanganese crusts: The "element perspective". Earth Planet Sc Lett 241, 952-961.

Bau, M., Koschinsky, A., 2009. Oxidative scavenging of cerium on hydrous Fe oxide: Evidence from the distribution of rare earth elements and yttrium between Fe oxides and Mn oxides in hydrogenetic ferromanganese crusts. Geochem J 43, 37-47.

Bau, M., Koschinsky, A., Dulski, P., Hein, J.R., 1996. Comparison of the partitioning behaviours of yttrium, rare earth elements, and titanium between hydrogenetic marine ferromanganese crusts and seawater. Geochim Cosmochim Ac 60, 1709-1725.

Bau, M., Moller, P., Dulski, P., 1997. Yttrium and lanthanides in eastern Mediterranean seawater and their fractionation during redox-

cycling. Mar Chem 56, 123-131.

Bau, M., Schmidt, K., Koschinsky, A., Hein, J., Kuhn, T., Usui, A., 2014. Discriminating between different genetic types of marine ferro-manganese crusts and nodules based on rare earth elements and yttrium. Chem Geol 381, 1-9.

Bidoglio, G., Gibson, P.N., Ogorman, M., Roberts, K.J., 1993. X-Ray-Absorption Spectroscopy Investigation of Surface Redox Transformations of Thallium and Chromium on Colloidal Mineral Oxides. Geochim Cosmochim Ac 57, 2389-2394.

Bodei, S., Manceau, A., Geoffroy, N., Baronnet, A., Buatier, M., 2007. Formation of todorokite from vernadite in Ni-rich hemipelagic sediments. Geochim Cosmochim Ac 71, 5698-5716.

Bonatti, E., Kraemer, T., Rydell, H., 1972. Classification and genesis of submarine iron-manganese deposits. In:Horn,D.R. (Ed.), Papers froma Conference on Ferromanganese Deposits on the Ocean Floor. Natl. Sci. Found. pp. 149-166.

Byrne, R.H., Kim, K.H., 1990. Rare-Earth Element Scavenging in Seawater. Geochim Cosmochim Ac 54, 2645-2656.

Decarlo, E.H., Mcmurtry, G.M., 1992. Rare-Earth Element Geochemistry of Ferromanganese Crusts from the Hawaiian Archipelago, Central Pacific. Chem Geol 95, 235-250.

Dubinin, A.V., Sval'nov, V.N., Berezhnaya, E.D., Rimskaya-Korsakova, M.N., Demidova, T.P., 2013. Geochemistry of trace and minor elements in sediments and manganese micronodules from the Angola Basin. Lithol Miner Resour+ 48, 175-197.

Frank, M., O'Nions, R.K., Hein, J.R., Banakar, V.K., 1999. 60 Myr records of major elements and Pb-Nd isotopes from hydrogenous

ferromanganese crusts: Reconstruction of seawater paleochemistry. Geochim Cosmochim Ac 63, 1689-1708.

Garbe-Schonberg, C.D., McMurtry, G.M., 1994. In-situ micro-analysis of platinum and rare earths in ferromanganese crusts by laser ablation-ICP-MS (LAICPMS). Fresenius J Anal Chem 350, 264-271.

Glasby, G.P., Ren, X., Shi, X., Pulyaeva, I.A., 2007. Co-rich Mn crusts from the Magellan seamount cluster: the long journey through time. Geo-Mar Lett 27, 315-323.

Godfrey, L.V., Lee, D.C., Sangrey, W.F., Halliday, A.N., Salters, V.J.M., Hein, J.R., White, W.M., 1997. The Hf isotopic composition of ferromanganese nodules and crusts and hydrothermal manganese deposits: Implications for seawater Hf. Earth Planet Sc Lett 151, 91-105.

Gulbrandsen, A., 1966. Chemical composition of phosphorites of the Phosphoria Formation. Geochim Cosmochim Ac 30, 769-78.

Halbach, P., 1986. Processes Controlling the Heavy-Metal Distribution in Pacific Ferromanganese Nodules and Crusts. Geol Rundsch 75, 235-247.

Halbach, P., Kriete, C., Prause, B., Puteanus, D., 1989. Mechanisms to explain the platinum concentration in ferromanganese seamount crusts. Chem geol 76, 95-106.

Halbach, P., Puteanus, D., 1984. The influence of the carbonate dissolution rate of the growth and composition of Co-rich ferromanganese crusts from Central Pacific seamount areas. Earth Planet Sc Lett 68, 73-87

Hein, J.R., Conrad, T.A., Frank, M., Christl, M., Sager, W.W., 2012.

Copper-nickel-rich, amalgamated ferromanganese crust-nodule deposits from Shatsky Rise, NW Pacific. Geochem Geophy Geosy 13.

Hein, J.R., Koschinsky, A.,2014. Deep-Ocean ferromanganese crusts and nodules. In: Scott, S. (Ed.), The Treatise on Geochemistry v.13. Elsevier.

Hein, J.R., Koschinsky, A., Halliday, A.N., 2003. Global occurrence of tellurium-rich ferromanganese crusts and a model for the enrichment of tellurium. Geochim Cosmochim Ac 67, 1117-1127.

Hein, J.R., Morgan, C.L., 1999. Influence of substrate rocks on Fe-Mn crust composition. Deep-Sea Res Pt I 46, 855-875.

Hein, J.R., Schwab, W.C., Davis, A.S., 1988. Cobalt-Rich and Platinum-Rich Ferromanganese Crusts and Associated Substrate Rocks from the Marshall-Islands. Mar Geol 78, 255-283.

Hein, J.R., Yeh, H.W., Gunn, S.H., Sliter, W.V., Benninger, L.M., Wang, C.H., 1993. 2 Major Cenozoic Episodes of Phosphogenesis Recorded in Equatorial Pacific Seamount Deposits. Paleoceanography 8, 293-311.

Horner, T.J., Schonbachler, M., Rehkamper, M., Nielsen, S.G., Williams, H., Halliday, A.N., Xue, Z., Hein, J.R., 2010. Ferromanganese crusts as archives of deep water Cd isotope compositions. Geochem Geophy Geosy 11.

Hyeong, K., Kim, J., Yoo, C.M., Moon, J.W., Seo, I., 2013. Cenozoic history of phosphogenesis recorded in the ferromanganese crusts of central and western Pacific seamounts: Implications for deepwater circulation and phosphorus budgets. Palaeogeogr Palaeocl 392, 293-301.

Jeong, K.S., Jung, H.S., Kang, J.K., Morgan, C.L., Hein, J.R., 2000. Formation of ferromanganese crusts on northwest intertropical Pacific seamounts: electron photomicrography and microprobe chemistry. Mar Geol 162, 541-559.

Klemm, V., Levasseur, S., Frank, M., Hein, J.R., Halliday, A.N., 2005. Osmium isotope stratigraphy of a marine ferromanganese crust. Earth Planet Sc Lett 238, 42-48.

Koschinsky, A., Halbach, P., 1995. Sequential leaching of marine ferromanganese precipitates: Genetic implications. Geochim Cosmochim Ac 59, 5113~5132.

Koschinsky, A., Halbach, P., Hein, J.R., Mangini, A., 1996. Ferromanganese crusts as indicators for paleoceanographic events in the NE Atlantic. Geol Rundsch 85, 567-576.

Koschinsky, A., Hein, J.R., 2003. Uptake of elements from seawater by ferromanganese crusts: solid-phase associations and seawater speciation. Mar Geol 198, 331-351.

Koschinsky, A., Stascheit, A., Bau, M., Halbach, P., 1997. Effects of phosphatization on the geochemical and mineralogical composition of marine ferromanganese crusts. Geochim Cosmochim Ac 61, 4079-4094.

Kuhn, T., Bau, M., Blum, N., Halbach, P., 1998. Origin of negative Ce anomalies in mixed hydrothermal-hydrogenetic Fe-Mn crusts from the Central Indian Ridge. Earth Planet Sc Lett 163, 207-220.

Kuhn, T., Bostick, B.C., Koschinsky, A., Halbach, P., Fendorf, S., 2003. Enrichment of Mo in hydrothermal Mn precipitates: possible Mo sources, formation process and phase associations. Chem Geol 199, 29-43.

Ling, H.F., Burton, K.W., ONions, R.K., Kamber, B.S., von Blanckenburg, F., Gibb, A.J., Hein, J.R., 1997. Evolution of Nd and Pb isotopes in Central Pacific seawater from ferromanganese crusts. Earth Planet Sc Lett 146, 1-12.

Little, S.H., Sherman, D.M., Vance, D., Hein, J.R., 2014. Molecular controls on Cu and Zn isotopic fractionation in Fe-Mn crusts. Earth Planet Sc Lett 396, 213-222.

Loges, A., Wagner, T., Barth, M., Bau, M., Gob, S., Markl, G., 2012. Negative Ce anomalies in Mn oxides: The role of Ce4+ mobility during water-mineral interaction. Geochim Cosmochim Ac 86, 296-317.

Mcarthur, J.M., Walsh, J.N., 1984. Rare-Earth Geochemistry of Phosphorites. Chem Geol 47, 191-220.

Mcclellan, G.H., 1980. Mineralogy of Carbonate Fluorapatites. J Geol Soc London 137, 675-681.

Murray, J.W., Dillard, J.G., 1979. Oxidation of Cobalt(Ii) Adsorbed on Manganese-Dioxide. Geochim Cosmochim Ac 43, 781-787.

Nathan, Y., 1984. The mineralogy and geochemistry of phosphorites. In *Phosphate Minerals* (ed. J. O. Nriagu and P. B. Moore), pp. 275-288. Springer Verlag.

Ohta, A., Kawabe, I., 2001. REE(Ⅲ) adsorption onto Mn dioxide (δ-MnO_2) and Fe oxyhydroxide: Ce(Ⅲ) oxidation by δ-MnO_2. Geochim Cosmochim Ac 65, 695-703.

Pan, J., De Carlo, E.H., Yang, Y., Liu, S., You, G., 2005. Effect of phosphatization on element concentration of cobalt-rich ferromanganese crusts. Ac geol sin 3, 349-355.

Peacock, C.L., Sherman, D.M., 2007. Crystal-chemistry of Ni in marine

ferromanganese crusts and nodules. Am Mineral 92, 1087-1092.

Piper, D.Z., Perkins, R.B., 2014. Geochemistry of a marine phosphate deposit: a signpost to phosphogenesis. In: Scott, S. (Ed.), The Treatise on Geochemistry v.13. Elsevier.

Puteanus, D., Halbach, P., 1988. Correlation of Co concentration and growth rate - A method for age determination of ferromanganese crusts. Chem geol 69, 73-85.

Schmidt, K., Bau, M., Hein, J.R., Koschinsky, A., 2014. Fractionation of the geochemical twins Zr-Hf and Nb-Ta during scavenging from seawater by hydrogenetic ferromanganese crusts. Geochim Cosmochim Ac 140, 468-487.

Takahashi, Y., Manceau, A., Geoffroy, N., Marcus, M.A., Usui, A., 2007. Chemical and structural control of the partitioning of Co, Ce, and Pb in marine ferromanganese oxides. Geochim Cosmochim Ac 71, 984-1008.

Wang, X.H., Muller, W.E.G., 2009. Marine biominerals: perspectives and challenges for polymetallic nodules and crusts. Trends Biotechnol 27, 375-383.

Wang, X.H., Peine, F., Schmidt, A., Schroder, H.C., Wiens, M., Schlossmacher, U., Muller, W.E.G., 2011. Concept of Biogenic Ferromanganese Crust Formation: Coccoliths as Bio-seeds in Crusts from Central Atlantic Ocean (Senghor Seamount/Cape Verde). Nat Prod Commun 6, 679-688.

Wang, X.H., Schlossmacher, U., Natalio, F., Schroder, H.C., Wolf, S.E., Tremel, W., Muller, W.E.G., 2009. Evidence for biogenic processes during formation of ferromanganese crusts from the Pacific Ocean: Implications of biologically induced mineralization. Micron 40, 526-535.

Wen, X., De Carlo, E.H., Li, Y.H., 1997. Interelement relationships in ferromanganese crusts from the central Pacific ocean: Their implications for crust genesis. Mar Geol 136, 277-297.

Zhang, J., Nozaki, Y., 1996. Rare earth elements and yttrium in seawater: ICP-MS determinations in the East Caroline, Coral Sea, and South Fiji basins of the western South Pacific Ocean. Geochim Cosmochim Ac 60, 4631-4644.

Table 1. Sampling information

Sample	On Bottom		Off Bottom		Depth (m)
	Latitude (N)	Longitude (E)	Latitude (N)	Longitude (E)	
Lemkein 99-1 **CD 1-5**	9° 19.528′	166° 08.083′	9° 20.002′	166° 07.477′	3225 – 2211
Lemkein 99-1 **CD 5-5**	9° 27.913′	166° 04.994′	9° 25.023′	166° 03.928′	2350 - 1559

Table 2. SEM-EDS data of non-phosphatized ferromanganese crusts CD 1-5 from the Lemkein seamount

Main phase	Mn (wt %)	Fe (wt %)	Mn/Fe	Si (wt %)	Ca (wt %)	# of Point	Texture
1-ver	32-37	12-15	2.4-2.6	0-2	3-4	3	C, L, Ma
2-ver (Fig. 3-b)	33-41	13-18	1.9-3.2	1-2	4	3	C, Ma
2-Fe (Fig. 3-b)	0-22	20-37	0-1.1	8-17	0-3	2	
3-ver (Fig. 3-a)	35-43	12-15	2.5-3.3	3-4	3-4	3	C, L
3-Fe (Fig. 3-a)	25	17	1.5	4	3	1	
4-ver	32-42	8-18	2.0-5.1	3-4	3-4	8	C, L
4-Fe	33	33	1.0	12	0	1	
5-ver (Fig. 3-c)	27-34	21-24	1.1-1.6	2-3	3-4	3	B, Mo
5-Fe (Fig. 3-c)	0-7	23-48	0-0.3	3-20	0-1	3	
6-ver (Fig. 3-d)	12-32	14-27	1.2-2.6	3-16	3-4	6	B, L, Mo
6-Fe (Fig. 3-d)	0-30	20-37	0-1.5	5-20	0	4	

* Abbreviation: Fe-bearing vernadite (Ver) and Fe oxyhydroxide (Fe) in main phase. Botryoidal (B), columnar (C), laminated (L), massive (Ma), and mottled (Mo) in texture.

Table 3. SEM-EDS data of non-phosphatized ferromanganese crusts CD 5-5 from the Lemkein seamount

image	Main phase	Mn (wt %)	Fe (wt %)	Mn/Fe	Ca (wt %)	P (wt %)	Ca/P	Ni (wt %)	#
Fig. 4-c	ver	34-36	24-29	1.2-1.5	4	1	4.0-5.0		2
	tod	57	2	28.3	2			5	1
	CFA	1	1	1.6	36	15	2.4		1
Fig. 5-a	ver	34-47	13-27	1.3-3.7	2-5	0-1	5.0-9.1	1-3	8
	tod	43-60	0-13	3.4-19.2	1-2			3-6	13
	CFA	3-10	1-4	2.3-39	28-35	12-15	2.3-2.4	0	2
Fig. 5-b	ver	29-44	9-18	1.9-3.5	4-12	1-5	2.5-6.1	1	17
	CFA	3-33	1-13	2.4-3.4	13-33	5-14	2.2-2.7	1	9
Fig. 5-c	ver	27-41	13-20	1.7-2.7	5-15	1-5	2.7-5.8	1	36
	CFA	5-25	3-14	1.1-2.6	15-32	6-13	2.3-2.5	0	10
Fig. 5-d	ver	29-39	13-21	1.4-3.1	3	0-1	5.5-15.7	1	5
	tod	38	4	9.2	1	0	5.8	3	1
	CFA	0-8	0-3	1.4-2.5	28-37	12-15	2.4-2.5	0	3

Table 3. SEM-EDS data of non-phosphatized ferromanganese crusts CD 5-5 from the Lemkein seamount (continued)

Fig. 5-e	ver	35-38	9-13	2.9-3.8	2-4	0	5.0-9.8	1-4	3
	tod	40-46	2-3	14.9-28.6	1-2	0	25.4	3-4	2
	Fe	1-14	37-48	0-0.1	1-8	1-3	1.2-2.6	0	4
	CFA	1-4	0-9	0.2-5.1	30-40	4-16	2.1-11.2	0	6

* Blank is not detected or cannot be calculated data

** Abbreviation in main phase: Fe-bearing vernadite (ver), todorokite (tod), Fe-rich phase (Fe), and carbonate fluorapatite (CFA)

*** # is number of point

Table 4. Chemical composition of non-phosphatized ferromanganese crusts CD 1-5 from the Lemkein seamount

CD 1-5	np-1	np-2		np-1	np-2
Mn (wt%)	25.80	26.73	**La (ppm)**	208.9	285.3
Fe	21.16	17.37	**Ce**	703.8	853.6
Ca	2.64	2.63	**Pr**	47.9	43.5
P	0.36	0.33	**Nd**	176.7	199.2
Ti	1.46	0.02	**Sm**	43.2	36.7
Ni	0.38	0.42	**Eu**	11.7	10.1
Co	0.70	0.96	**Gd**	70.2	61.8
K	0.06	0.06	**Tb**	8.8	7.8
Sr	0.20	0.20	**Dy**	53.7	50.7
Pb	0.14	0.15	**Ho**	11.9	11.5
Ba	0.18	0.14	**Er**	35.3	35.1
Al	0.67	0.39	**Tm**	5.1	5.1
Zn (ppm)	618.5	550.4	**Yb**	33.7	34.0
V	765.3	710.7	**Lu**	5.3	5.3
Cu	628.6	573.0	**Mn/Fe**	1.22	1.54
As	216.6	217.6	**Ca/P**	7.31	7.84
Y	180.1	226.4	**Y/Ho**	15.20	19.65

* Mn to Al are [wt%] and Zn to Lu are [ppm]

Table 5. Chemical composition of ferromanganese crusts CD 5-5 from the Lemkein seamount

CD5-5	C0	C1	L1	R1	C2	L2	R2-1	R2-2	C3	R3	np
Mn (wt%)	27.71	23.05	25.43	27.73	26.21	25.07	26.12	26.68	25.74	25.65	31.17
Fe	9.87	7.74	8.02	7.45	6.79	6.25	6.47	6.56	5.57	6.75	16.08
Ca	11.49	12.52	11.44	10.75	9.85	12.15	12.18	12.94	12.75	13.00	2.61
P	3.54	3.97	3.51	3.36	3.95	4.11	3.94	4.08	4.06	4.18	0.42
Mg	1.08	0.95	1.04	1.14	1.05	1.13	1.09	1.06	1.08	1.01	1.28
Ti	0.61	0.45	0.43	0.40	0.39	0.35	0.36	0.39	0.33	0.41	1.02
Ni	0.64	0.61	0.67	0.82	0.80	0.85	0.80	0.77	0.87	0.73	0.56
Co	0.33	0.30	0.32	0.37	0.36	0.34	0.33	0.33	0.33	0.31	1.54
K	0.30	0.22	0.36	0.42	0.42	0.46	0.43	0.42	0.45	0.41	0.49
Sr	0.23	0.21	0.20	0.20	0.18	0.18	0.18	0.20	0.18	0.20	0.17
Pb	0.19	0.17	0.16	0.17	0.17	0.15	0.14	0.14	0.15	0.14	0.19
Ba	0.20	0.17	0.17	0.19	0.17	0.17	0.11	0.12	0.16	0.16	0.14
Al	0.13	0.12	0.12	0.11	0.09	0.10	0.09	0.09	0.09	0.08	0.31
Zn (ppm)	771.3	749.1	746.0	1005.2	923.5	1013.0	955.2	935.3	955.8	895.8	600.5
V	619.8	487.6	517.6	570.1	502.5	504.6	503.1	518.4	462.3	514.4	642.4
Cu	608.8	457.5	632.0	593.2	453.2	523.5	447.4	483.3	414.3	415.3	414.5
Tl	189.7	163.5	133.7	172.0	228.6	219.5	140.8	136.9	154.0	140.5	242.2
As	171.9	120.1	138.0	142.3	125.7	125.9	134.6	147.1	123.1	144.6	289.1
Y	149.8	170.1	110.4	130.7	49.4	91.6	123.7	244.6	238.0	149.5	146.4
U	11.3	9.3	9.7	9.1	8.9	8.2	8.5	9.4	8.3	9.8	15.1

Table 5. Chemical composition of ferromanganese crusts CD 5-5 from the Lemkein seamount (continued)

Cd	5.6	5.1	5.6	6.9	6.8	6.8	6.5	6.3	7.1	6.0	6.5
Th	10.9	9.1	6.6	4.0	2.2	2.9	3.4	2.1	2.3	2.5	3.1
Pt	0.4	0.3	0.5	0.3	0.6	0.3	0.3	0.2	0.4	0.2	0.5
La	98.3	157.3	136.7	122.6	56.3	75.9	94.8	152.3	131.5	129.7	165.8
Ce	1643.8	692.6	1212.4	1352.6	1243.3	1142.0	1296.0	1279.5	1207.6	1306.8	699.4
Pr	26.1	25.7	21.0	19.7	12.9	15.8	20.3	20.8	20.0	19.2	23.2
Nd	105.1	105.9	85.8	81.6	53.3	65.6	84.8	88.0	84.9	79.4	122.0
Sm	21.2	21.4	17.3	15.8	10.4	12.7	16.1	16.4	16.1	15.6	21.4
Eu	5.5	5.6	4.5	4.3	2.9	3.5	4.3	4.5	4.5	4.3	5.9
Gd	25.1	26.0	21.5	21.1	12.6	17.3	22.6	23.3	22.5	20.7	36.5
Tb	3.9	4.0	3.4	3.3	1.9	2.7	3.4	3.5	3.4	3.2	4.6
Dy	23.1	23.8	20.2	20.5	11.5	16.7	21.5	22.1	21.6	19.5	30.1
Ho	5.2	5.4	4.8	5.0	2.7	4.0	5.2	5.4	5.3	4.6	7.0
Er	16.2	17.0	15.1	15.9	7.9	12.8	16.5	17.1	16.7	14.6	21.7
Tm	2.3	2.4	2.1	2.2	1.1	1.8	2.3	2.4	2.3	2.0	3.2
Yb	14.9	15.8	13.9	14.5	6.7	11.7	15.0	15.2	14.7	13.0	21.2
Lu	2.4	2.5	2.3	2.4	1.0	1.9	2.4	2.4	2.4	2.1	3.5
Mn/Fe	2.81	2.98	3.17	3.72	3.86	4.01	4.04	4.07	4.62	3.80	1.94
Ca/P	3.25	3.15	3.26	3.20	2.49	2.96	3.09	3.17	3.14	3.11	6.27
Y/Ho	28.81	31.50	23.00	26.14	18.30	22.90	23.79	45.30	44.91	32.50	20.81

* Mn to Al are [wt%] and Zn to Lu are [ppm].

** CD 5-5 np is a non-phosphatized crust sample. Others are phosphatized crusts samples

Table 6. Correlation coefficients of ten bulk analyses of phosphatized crust CD 5-5 from the Lemkein seamount

	REE	Ce	Y	Cd	Tl	Th	U	Pt	Cu	As	V	Ba	Mg
REE	1.00												
Ce	-0.22	1.00											
Y	0.74	-0.06	1.00										
Cd	-0.60	0.27	-0.06	1.00									
Tl	-0.74	0.05	-0.61	0.31	1.00								
Th	0.49	-0.02	-0.03	-0.79	0.01	1.00							
U	0.37	0.47	0.06	-0.67	-0.12	0.71	1.00						
Pt	-0.50	0.09	-0.53	0.08	0.46	0.15	0.02	1.00					
Cu	0.11	0.38	-0.27	-0.26	0.09	0.54	0.49	0.25	1.00				
As	0.24	0.80	0.13	-0.29	-0.15	0.41	0.84	-0.17	0.52	1.00			
V	0.09	0.70	-0.15	-0.24	0.16	0.54	0.77	-0.02	0.72	0.88	1.00		
Ba	-0.07	0.11	-0.29	-0.18	0.49	0.51	0.43	0.40	0.50	0.19	0.46	1.00	
Mg	-0.41	0.56	-0.15	0.75	0.30	-0.33	-0.29	0.01	0.35	0.18	0.31	0.03	1.00
Mn	-0.19	0.92	0.00	0.41	0.07	-0.11	0.34	0.06	0.40	0.71	0.70	0.09	0.66
Fe	0.30	0.33	-0.18	-0.68	0.08	0.89	0.89	0.20	0.71	0.69	0.82	0.56	-0.17
Ni	-0.55	0.18	0.00	0.98	0.22	-0.85	-0.75	-0.02	-0.35	-0.36	-0.36	-0.30	0.70
Co	-0.64	0.41	-0.38	0.77	0.56	-0.41	-0.29	0.29	0.22	0.01	0.26	0.17	0.77
Al	0.35	-0.04	-0.14	-0.56	0.16	0.89	0.53	0.32	0.75	0.28	0.54	0.65	-0.08

*REE indicates sum of La, Pr, Nd, Sm, Eu, Gd, Tb, Dy, Ho, Er, Tm, Yb, and Lu.

Table 6. Correlation coefficients of ten bulk analyses of phosphatized crust CD 5-5 from the Lemkein seamount (continued)

	REE	Ce	Y	Cd	Tl	Th	U	Pt	Cu	As	V	Ba	Mg
K	-0.56	0.36	-0.05	0.90	0.08	-0.88	-0.59	-0.06	-0.23	-0.16	-0.25	-0.35	0.70
Zn	-0.50	0.18	-0.02	0.91	0.24	-0.82	-0.68	-0.27	-0.32	-0.25	-0.21	-0.32	0.71
Ti	0.34	0.38	-0.02	-0.68	0.07	0.87	0.94	0.12	0.54	0.76	0.79	0.52	-0.24
Pb	0.03	0.21	-0.27	-0.30	0.43	0.72	0.58	0.55	0.61	0.35	0.63	0.83	-0.01
Sr	0.63	0.18	0.21	-0.79	-0.20	0.82	0.90	-0.23	0.45	0.70	0.70	0.39	-0.37
P	-0.16	-0.38	0.25	0.16	0.00	-0.52	-0.45	-0.34	-0.86	-0.45	-0.70	-0.50	-0.31
Ca	0.61	-0.26	0.73	-0.21	-0.61	-0.09	-0.08	-0.75	-0.45	-0.03	-0.36	-0.45	-0.29
Ca/P	0.86	0.11	0.59	-0.42	-0.71	0.44	0.38	-0.51	0.39	0.44	0.31	0.01	-0.01
Mn/Fe	-0.34	0.03	0.26	0.85	-0.05	-0.91	-0.76	-0.16	-0.60	-0.43	-0.58	-0.51	0.43

Table 6. Correlation coefficients of ten bulk analyses of phosphatized crust CD 5-5 from the Lemkein seamount (continued)

	Mn	Fe	Ni	Co	Al	K	Zn	Ti	Pb	Sr	P	Ca	Ca/P	Mn/Fe
Mn	1.00													
Fe	0.26	1.00												
Ni	0.29	-0.79	1.00											
Co	0.64	-0.16	0.65	1.00										
Al	-0.01	0.82	-0.65	-0.09	1.00									
K	0.41	-0.72	0.93	0.59	-0.72	1.00								
Zn	0.33	-0.72	0.94	0.68	-0.65	0.87	1.00							
Ti	0.26	0.96	-0.78	-0.25	0.71	-0.71	-0.71	1.00						
Pb	0.26	0.79	-0.47	0.22	0.84	-0.55	-0.49	0.73	1.00					
Sr	0.13	0.87	-0.84	-0.40	0.64	-0.77	-0.69	0.90	0.55	1.00				
P	-0.50	-0.68	0.30	-0.33	-0.74	0.26	0.29	-0.50	-0.72	-0.43	1.00			
Ca	-0.38	-0.32	-0.06	-0.70	-0.35	-0.02	-0.02	-0.17	-0.64	0.10	0.59	1.00		
Ca/P	0.08	0.35	-0.38	-0.46	0.38	-0.30	-0.33	0.34	0.02	0.56	-0.36	0.54	1.00	
Mn/Fe	0.10	-0.92	0.92	0.36	-0.82	0.87	0.83	-0.85	-0.69	-0.83	0.54	0.24	-0.29	1.00

Table 7. REY and major elements correlation coefficients of ten bulk analyses of phosphatized crust CD 5-5 from the Lemkein seamount

	La	Ce	Pr	Nd	Sm	Eu	Gd	Tb	Dy	Ho	Er	Tm	Yb	Lu
La	1.00													
Ce	-0.36	1.00												
Pr	0.64	-0.04	1.00											
Nd	0.68	-0.07	1.00	1.00										
Sm	0.64	-0.09	1.00	0.99	1.00									
Eu	0.68	-0.09	0.99	0.99	0.99	1.00								
Gd	0.75	-0.08	0.95	0.97	0.93	0.96	1.00							
Tb	0.75	-0.07	0.96	0.98	0.95	0.97	0.99	1.00						
Dy	0.76	-0.05	0.92	0.94	0.89	0.92	0.99	0.99	1.00					
Ho	0.77	-0.03	0.83	0.87	0.80	0.84	0.96	0.94	0.98	1.00				
Er	0.77	-0.04	0.81	0.85	0.78	0.82	0.94	0.93	0.98	1.00	1.00			
Tm	0.76	-0.04	0.83	0.87	0.80	0.83	0.95	0.94	0.98	1.00	1.00	1.00		
Yb	0.76	-0.06	0.84	0.87	0.81	0.84	0.95	0.95	0.98	0.99	0.99	1.00	1.00	
Lu	0.75	-0.03	0.82	0.85	0.79	0.82	0.93	0.94	0.97	0.98	0.99	0.99	1.00	1.00
Y	0.75	-0.06	0.52	0.58	0.48	0.56	0.69	0.64	0.72	0.77	0.76	0.75	0.70	0.68
Mn	-0.28	0.92	-0.09	-0.10	-0.14	-0.13	-0.10	-0.09	-0.06	-0.01	-0.01	-0.02	-0.04	-0.02
Fe	0.05	0.33	0.63	0.56	0.64	0.58	0.39	0.44	0.32	0.18	0.15	0.19	0.21	0.21

Table 7. REY and major elements correlation coefficients of ten bulk analyses of phosphatized crust CD 5-5 from the Lemkein seamount (continued)

	La	Ce	Pr	Nd	Sm	Eu	Gd	Tb	Dy	Ho	Er	Tm	Yb	Lu
P	-0.02	-0.38	-0.32	-0.28	-0.32	-0.27	-0.18	-0.24	-0.18	-0.16	-0.14	-0.15	-0.19	-0.24
Ca	0.62	-0.26	0.40	0.45	0.38	0.44	0.59	0.56	0.61	0.65	0.67	0.66	0.63	0.61
Ca/P	0.73	0.11	0.79	0.81	0.77	0.79	0.87	0.90	0.90	0.91	0.92	0.91	0.93	0.95
Mn/Fe	-0.15	0.03	-0.61	-0.55	-0.65	-0.58	-0.37	-0.43	-0.29	-0.13	-0.11	-0.15	-0.19	-0.18

	Y	Mn	Fe	P	Ca	Ca/P	Mn/Fe
Y	1.00						
Mn	0.00	1.00					
Fe	-0.18	0.26	1.00				
P	0.25	-0.50	-0.68	1.00			
Ca	0.73	-0.38	-0.32	0.59	1.00		
Ca/P	0.59	0.08	0.35	-0.36	0.54	1.00	
Mn/Fe	0.26	0.10	-0.92	0.54	0.24	-0.29	1.00

Table 8. Simplified correlation coefficient, CC #* table

CC 90		Mn	Fe	Ca	P	Co	Mg	Ce	V	As	K	Ni	Zn	Cd	Cu	Ti	Al	Sr	Pb	U	Th	Tl	Pt	REE	Y	Ba
Crust	Mn	1						+																		
	Fe		1													+										
	Mn/Fe		-									+									-					
CFA	Ca			1																						
	P				1																					
	Ca/P																									

CC 80		Mn	Fe	Ca	P	Co	Mg	Ce	V	As	K	Ni	Zn	Cd	Cu	Ti	Al	Sr	Pb	U	Th	Tl	Pt	REE	Y	Ba
Crust	Mn	1						+																		
	Fe		1						+							+	+	+		+	+					
	Mn/Fe		-								+	+	+	+		-	-				-					
CFA	Ca			1																						
	P				1										-											
	Ca/P																							+		

CC 60		Mn	Fe	Ca	P	Co	Mg	Ce	V	As	K	Ni	Zn	Cd	Cu	Ti	Al	Sr	Pb	U	Th	Tl	Pt	REE	Y	Ba
Crust	Mn	1				+	+	+	+	+																
	Fe		1		-				+	+	-	-	-	-	+	+	+	+	+	+	+					
	Mn/Fe		-								+	+	+	+	-	-	-	-	-	-	-					
CFA	Ca			1		-													-			-	-	+	+	
	P		-		1				-						-		-		-							
	Ca/P																					-		+		

* CC # indicates correlation coefficients over the specific absolute value. (e.g. CC 90 shows positive or negative correlations that have value over |0.90|)

Table 9. EPMA data of phosphatized crust CD5-5 from the Lemkein seamount

point	SiO2	Al2O3	Fe2O3	MnO2	MgO	CaO	Na2O	SO3	P2O5	NiO	K2O	CeO2	Total
todo	0.06	3.36	4.36	63.51	6.84	1.43	0.85	0.10	0.13	4.70	1.12	0.25	86.71
todo	0.00	3.34	4.26	63.82	6.72	1.49	0.80	0.21	0.29	4.53	1.06	0.20	86.70
todo	0.48	3.08	5.99	63.60	6.00	1.78	0.92	0.26	0.18	4.31	0.92	0.12	87.63
todo	0.36	3.09	6.32	65.09	6.14	1.78	0.83	0.17	0.47	4.53	0.92	0.12	89.81
todo	0.52	3.20	6.06	63.42	6.22	1.79	0.90	0.08	0.11	4.68	0.81	0.22	88.00
todo	0.44	3.27	5.95	63.68	6.20	1.72	0.85	0.36	0.09	4.50	0.86	0.08	88.00
ver	1.04	0.61	12.49	59.71	2.40	3.71	1.04	0.45	0.39	1.20	0.95	0.21	84.19
ver	0.67	1.15	10.68	60.91	3.66	3.49	1.03	0.27	0.32	1.98	0.92	0.18	85.24
ver	0.66	1.78	9.20	59.88	4.78	3.14	1.10	0.29	0.25	2.54	0.94	0.25	84.81
ver	0.87	0.60	12.09	61.14	2.81	3.56	1.11	0.36	0.28	1.22	0.93	0.26	85.24
ver	0.98	0.69	11.90	60.88	2.81	3.56	1.13	0.54	0.34	1.38	0.96	0.22	85.37
ver	0.91	0.55	12.20	60.22	2.51	3.79	1.12	0.78	0.49	1.24	0.94	0.22	84.96
fibber-todo	0.24	1.77	5.87	63.24	5.24	2.23	0.79	0.29	0.04	3.72	1.22	0.09	84.73
fibber-todo	0.00	1.89	3.46	64.66	5.88	2.01	1.04	0.20	0.09	5.87	0.88	0.13	86.12

Table 9. EPMA data of phosphatized crust CD5-5 from the Lemkein seamount (continued)

point	SiO2	Al2O3	Fe2O3	MnO2	MgO	CaO	Na2O	SO3	P2O5	NiO	K2O	CeO2	Total
fibber-todo	0.00	0.26	0.83	70.37	4.26	1.70	1.03	0.04	0.00	4.95	2.06	0.10	85.59
CFA	0.00	0.00	0.86	2.00	0.21	51.40	0.72	1.80	29.58	0.07	0.05	0.02	86.70
CFA	0.39	0.02	6.06	13.19	0.57	44.00	0.90	1.62	19.63	0.23	0.19	0.19	86.99

Table 10. Defocused beam data for LA-ICP-MS

	FeO	CaO	SiO2		FeO	CaO	SiO2
todo	4.93	1.48	0.27	**ver2**	9.37	14.35	0.82
todo	5.42	1.43	0.55	**ver2**	8.15	20.13	0.62
todo	4.64	1.37	0.41	**ver2**	9.50	14.70	0.84
todo	5.25	1.40	0.36	**CFAagg**	13.74	11.20	1.69
todo	5.43	1.75	0.00	**CFAagg**	11.94	14.69	1.42
todo	5.90	3.94	0.53	**CFAagg**	12.83	14.63	1.37
ver	8.12	2.55	0.66	**ver3**	12.04	8.65	1.29
ver	8.00	2.32	0.79	**ver3**	13.28	7.44	1.46
ver	8.42	2.87	0.72	**ver3**	12.46	7.44	1.40
ver2	9.78	15.41	0.87	**ver3**	13.21	7.25	1.25
ver2	11.08	9.70	1.14	**CFAagg**	11.35	18.10	1.39
ver2	8.72	17.35	0.74	**InsideCFA**	9.88	10.08	0.82
ver2	9.65	11.49	0.00	**InsideTod**	15.37	7.74	1.78

Table 11. LA-ICP-MS data of phosphatized crust CD5-5 from the Lemkein seamount

Element	Todo-1	Todo-2	Todo-3	ver-1-1	ver-1-2	ver-1-3
Si29	0.19	0.2	0.17	0.29	0.32	0.38
Ca43	1.06	1.02	0.98	1.82	1.66	2.05
Ca44	1.05	1.01	0.96	1.93	1.71	2.08
Fe56	3.82	4.21	3.75	6.9	7.08	8.32
Fe58	4.39	2.21	4.54	1.82	1.28	1.89
Cu65	2090.6	1157.08	2026.17	1106.25	880.81	1170.84
Y89	9.34	5.9	8.64	8.3	6.99	9.38
La139	18.81	14.01	18.3	16.8	15.54	19.12
Ce140	688.07	560.72	580.01	891.56	681.94	837.97
Pr141	2.22	1.45	2.23	1.86	1.64	2.17
Nd146	9.37	6.47	9.62	7.82	6.7	8.94

* Si, Ca, and Fe are [wt %], and the others are [ppm]

Table 11. LA-ICP-MS data of phosphatized crust CD5-5 from the Lemkein seamount (continued)

Element	ver-2-1	ver-2-2	ver-2-3	ver-2-4	ver-3-1	ver-3-2	ver-3-3
Si29	0.44	0.31	0.54	0.46	0.54	0.53	0.49
Ca43	11.01	6.93	10.26	10.51	5.32	6.18	5.32
Ca44	11.91	6.85	10.44	11.12	5.22	6.4	5.46
Fe56	10.66	7.36	13.1	10.7	12.47	12.36	12.17
Fe58	0.95	0.71	1.36	1.11	0.84	0.78	1.07
Cu65	617.61	469.47	904.95	778.41	479.96	468.58	604.37
Y89	108.73	63.61	105.19	124.17	143.06	246.7	151.19
La139	145.71	81.07	136.2	148.23	108.7	163.72	105.61
Ce140	586.92	365.32	697.73	662.25	1582.63	1530.35	1748.38
Pr141	21.87	13.46	20.49	21.31	19.47	34.19	19.24
Nd146	81.95	44.88	79.9	87.2	78.54	143.49	89.16

* Si, Ca, and Fe are [wt %], and the others are [ppm]

Table 11. LA-ICP-MS data of phosphatized crust CD5-5 from the Lemkein seamount (continued)

Element	Todo-1	Todo-2	Todo-3	ver-1-1	ver-1-2	ver-1-3
Sm147	1.89	1.24	2.05	1.38	1.26	1.41
Eu153	0.57	0.28	0.49	0.45	0.41	0.55
Gd157	3.8	2.25	3.19	3.37	2.95	3.52
Tb159	0.43	0.26	0.35	0.34	0.3	0.49
Dy163	2.87	1.81	2.78	3.12	2.46	3.14
Ho165	0.56	0.42	0.46	0.65	0.56	0.68
Er166	2.05	1.28	2.04	1.91	1.86	2.21
Tm169	0.27	0.21	0.31	0.31	0.3	0.36
Yb172	2.49	1.93	2.36	2.45	2.39	2.6
Lu175	0.45	0.24	0.38	0.39	0.32	0.47
Y/Ho	16.59	14.15	18.82	12.69	12.55	13.73
Ce_{SN}/Ce_{SN^*}	23.24	26.52	19.92	34.44	28.92	28.21

Table 11. LA-ICP-MS data of phosphatized crust CD5-5 from the Lemkein seamount (continued)

Element	ver-2-1	ver-2-2	ver-2-3	ver-2-4	ver-3-1	ver-3-2	ver-3-3
Sm147	15.35	8.94	16.27	17.62	16.33	29.95	17.78
Eu153	4.04	2.39	3.74	4.33	4.36	7.53	4.19
Gd157	19.31	11.15	20.24	21.11	22.33	37.18	24.45
Tb159	2.74	1.57	2.83	3.11	2.85	5.11	3.09
Dy163	19.25	12.02	20.85	22.24	22.05	35.95	23.24
Ho165	4.61	2.75	4.52	4.92	4.23	7.53	4.78
Er166	13.24	8.32	13.54	14.89	11.86	21.24	13.31
Tm169	2.22	1.14	2.02	2.16	1.9	3.04	2.01
Yb172	14.11	8.12	14.11	14.79	12.31	20.17	13.67
Lu175	2.26	1.28	2.07	2.16	1.87	3.01	1.99
Y/Ho	23.59	23.13	23.27	25.24	33.82	32.76	31.63
Ce_{SN}/Ce_{SN^*}	2.34	2.52	2.98	2.64	7.87	4.71	8.89

Table 11. LA-ICP-MS data of phosphatized crust CD5-5 from the Lemkein seamount (continued)

Element	inside CFA	inside Tod	CFA agg-1	CFA agg-2	CFA agg-3	Element	inside CFA	inside Tod	CFA agg-1	CFA agg-2	CFA agg-3
Si29	0.29	0.69	1.92	0.67	1.36	**Sm147**	46.51	10.2	24.69	42.07	19.92
Ca43	7.2	5.53	10.46	8	10.5	**Eu153**	11.44	2.81	6.01	10.68	5.79
Ca44	7.1	5.51	10.47	7.69	10.36	**Gd157**	70.2	12.12	37.34	54.98	31.5
Fe56	7.73	15.33	40.81	13.27	29.5	**Tb159**	9.59	2	4.53	7.9	4.16
Fe58	0.84	0.88	1.55	0.44	1.43	**Dy163**	72.33	14.72	32.03	58.02	29.47
Cu65	454.63	863.94	926.29	266.34	781.51	**Ho165**	16.51	3.31	6.35	11.9	6.33
Y89	776.33	69.47	205.05	370.33	202.37	**Er166**	48.32	9.66	18.65	35.77	18.71
La139	353.72	89.99	172.63	252.87	169.66	**Tm169**	6.56	1.38	2.9	4.9	2.74
Ce140	125.93	490.84	4713.16	1394.81	3830.4	**Yb172**	40.83	9.7	18.57	31.38	19.08
Pr141	49.32	14.08	29.31	49.94	27.83	**Lu175**	6.19	1.66	3.08	4.97	3
Nd146	233.93	55.51	122.44	218.51	110.85	**Y/Ho**	47.02	20.99	32.29	31.12	31.97
* Si, Ca, and Fe are [wt %], and the others are [ppm]						**CeSN/CeSN***	0.21	3.12	15.11	2.85	12.67

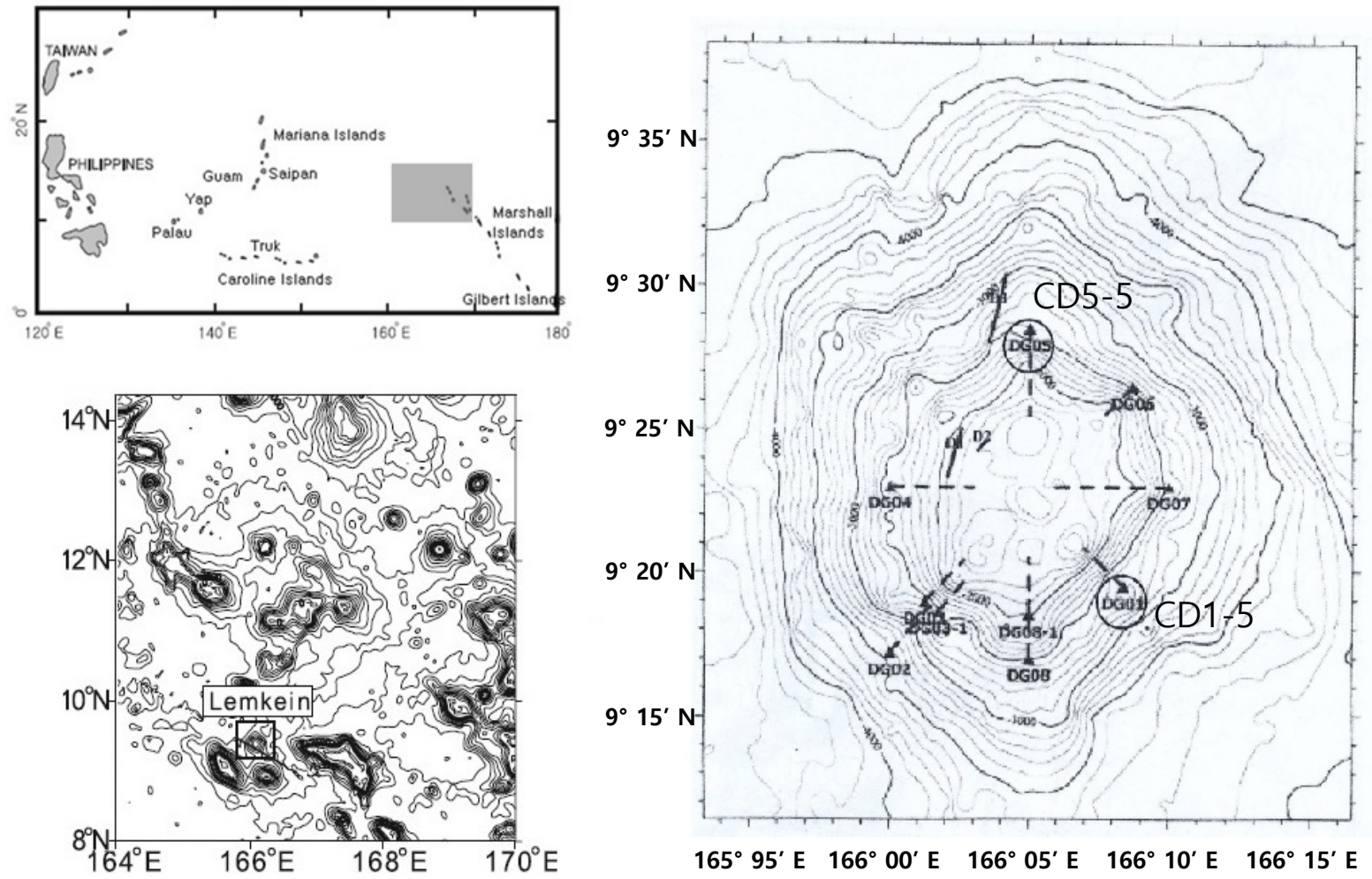

Figure 1. Location of the Lemkein seamount with dredged sampling sites (modified after Kim et al., 2006).

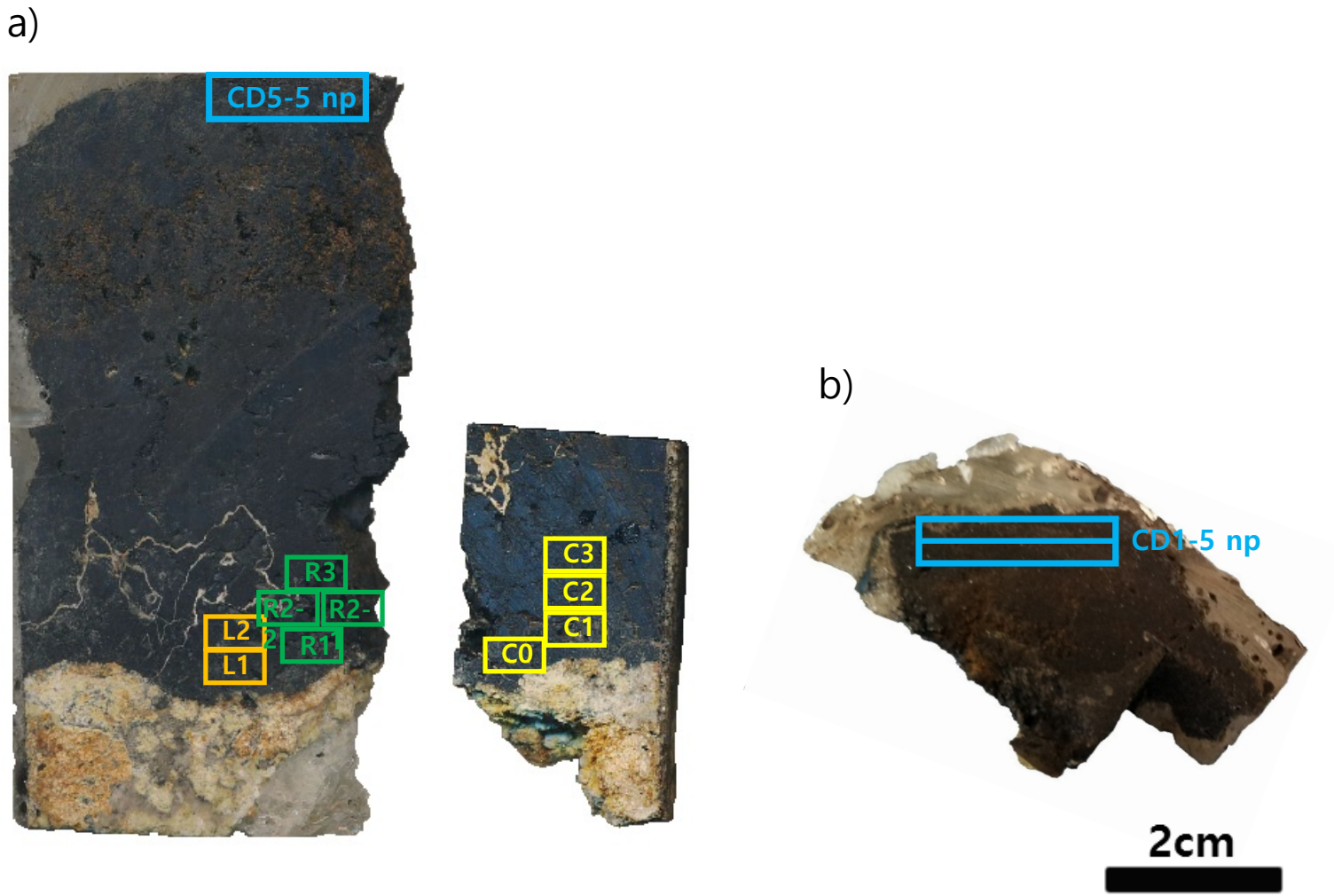

Figure 2. Lemkein 99-1 a) CD 5-5 and b) CD 1-5. Marked parts were sampled and quantitatively analyzed.

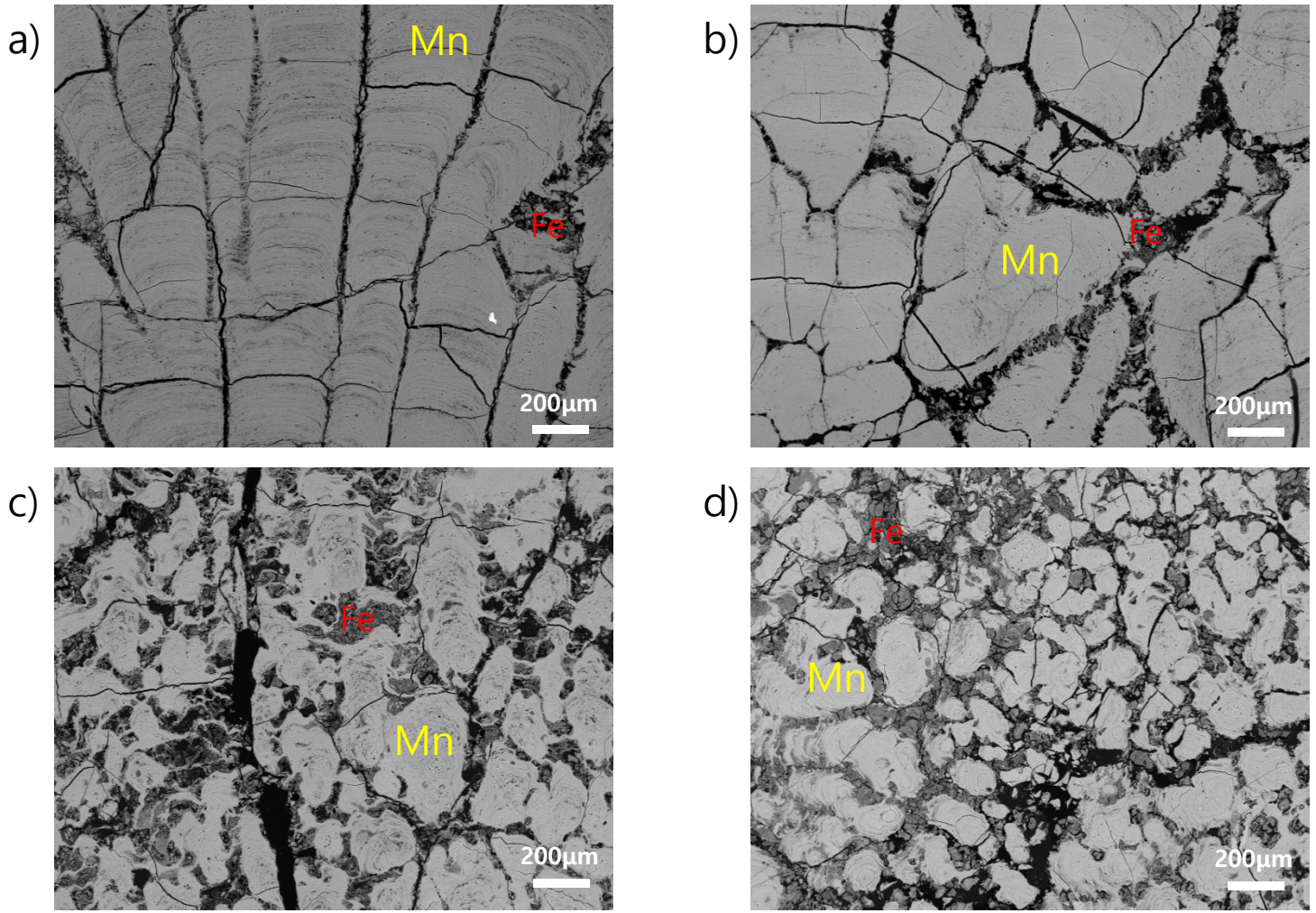

Figure 3. BSE images of non-phosphatized crust CD 1-5. a) laminated and columnar texture. b) massive and columnar texture of mainly Mn oxide. c ,d) columnar and botryoidal texture of Mn oxide mottled with Fe oxyhydroxide. Bright part represents Mn-rich phase and grey shaded part indicates Fe-rich phase. Main element is marked on BSE images.

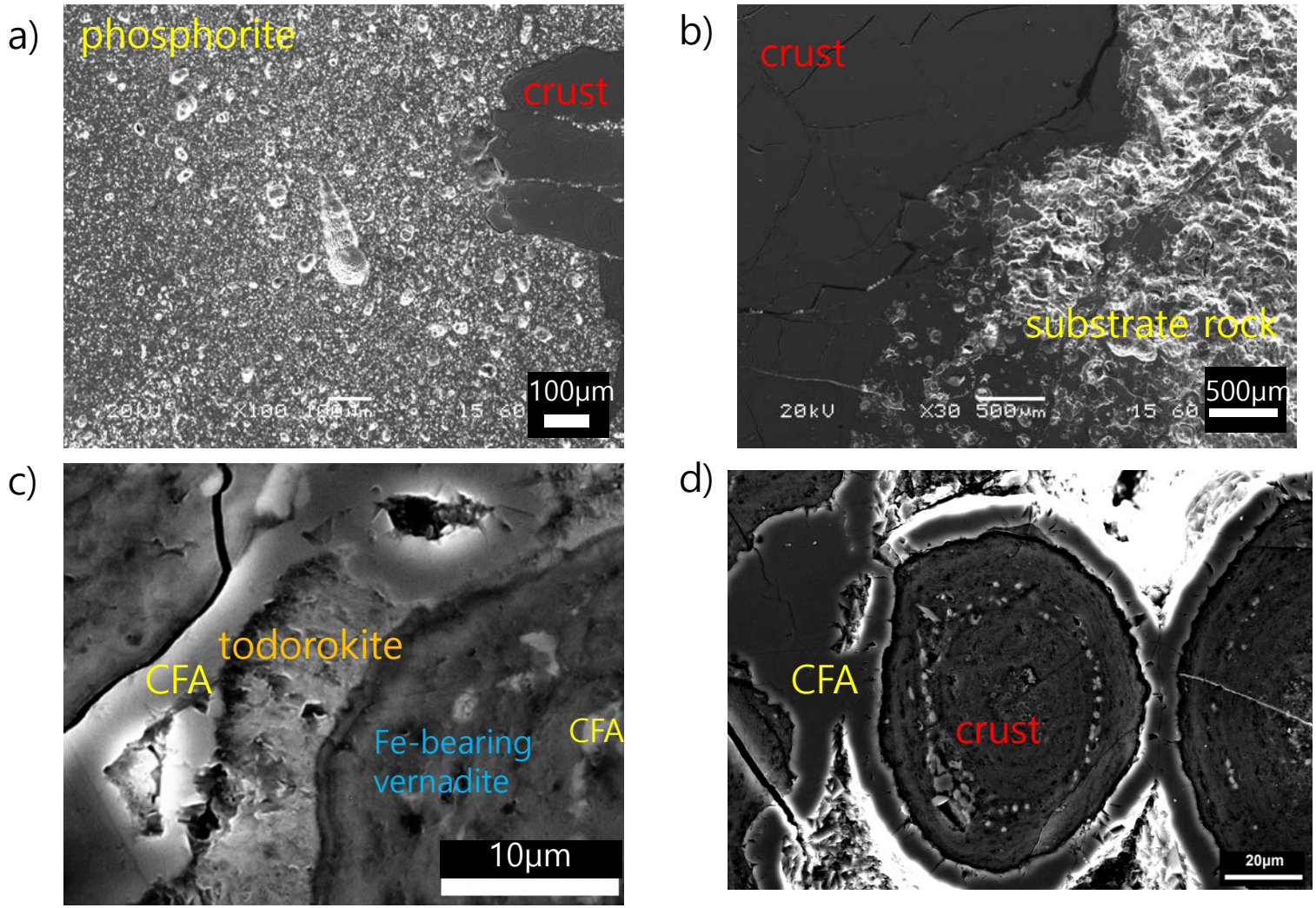

Figure 4. SEI images of phosphatized crust CD 5-5. a) Phosphorite with biogenic mold in phosphatized ferromanganese crusts. b) Boundary between substrate rock and ferromanganese crusts. c) Major minerals composing phosphatized crusts; CFA, todorokite, and Fe-bearing vernadite. d) phosphatized crusts enveloped and infilled by CFA.

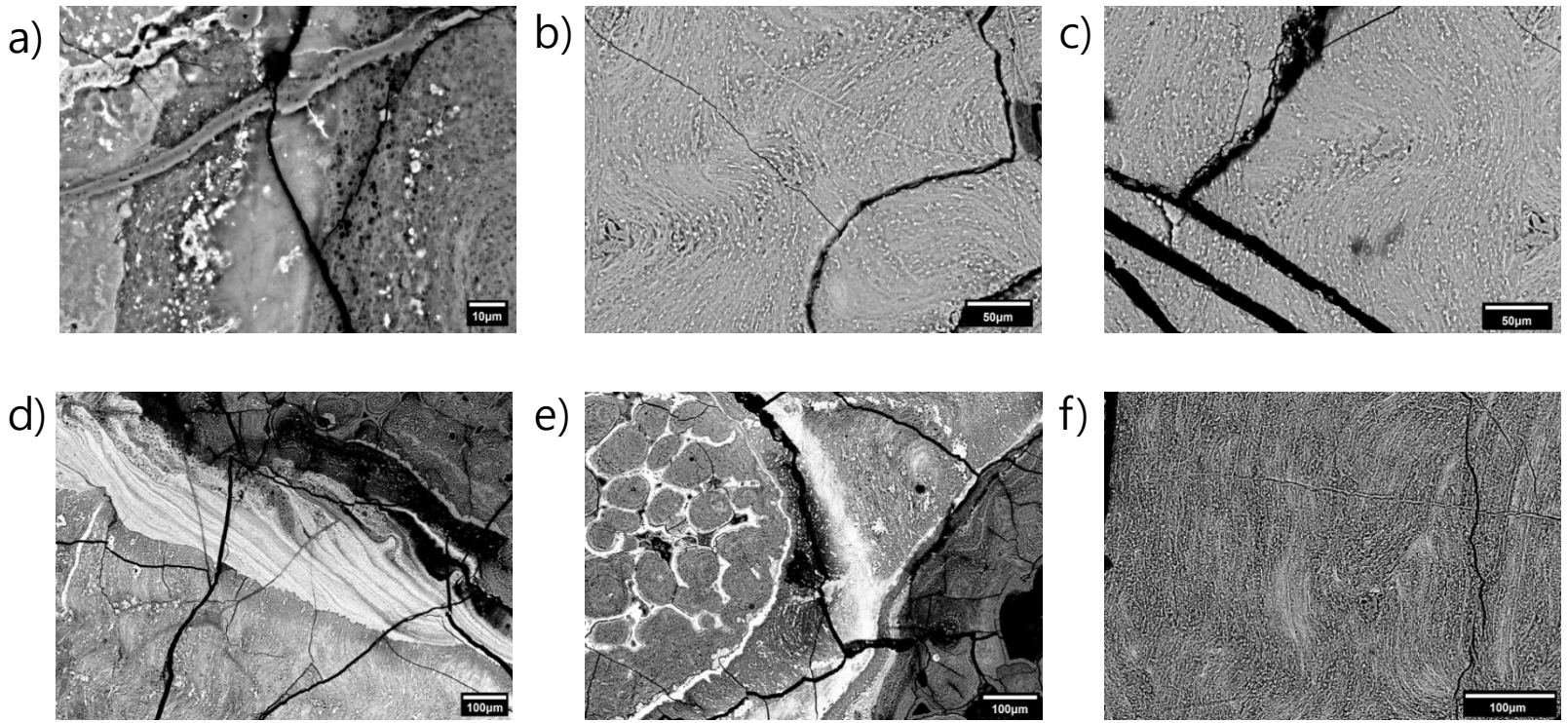

Figure 5. BSE images of phosphatized crust CD 5-5. (a, d, e) Fe-bearing vernadite, todorokite, and CFA constitute phosphatized ferromanganese crusts closed to phosphorite. (b, c, f) phosphatized ferromanganese crusts near the boundary between crust and substrate rock are composed of Fe-bearing vernadite and CFA.

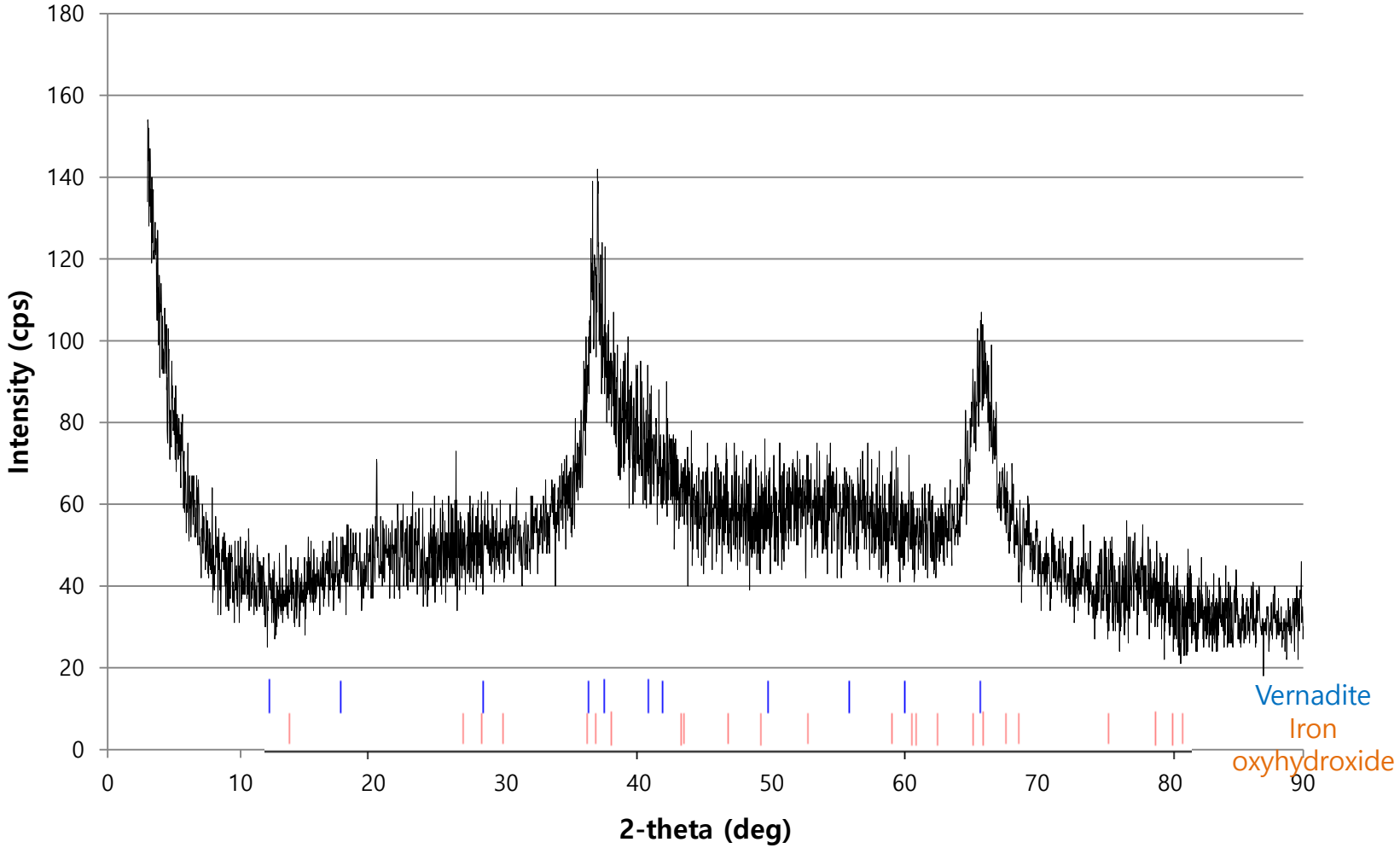

Figure 6. XRD result of non phosphatized layer CD 1-5. Major peaks are coincident with vernadite and iron oxyhydroxide peaks.

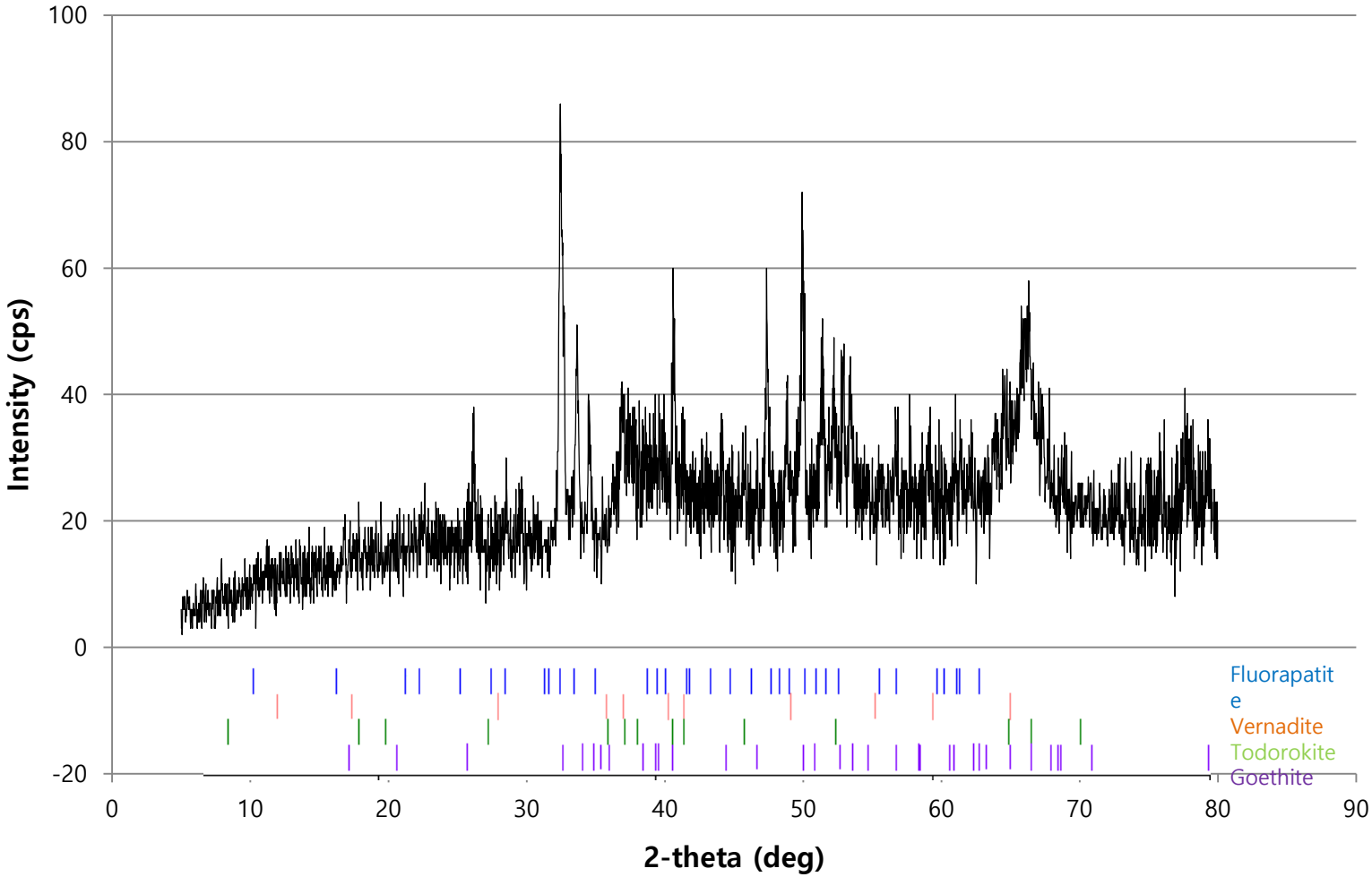

Figure 7. XRD result of phosphatized layer CD 5-5. Major peaks are coincident with fluorapatite, vernadite, todorokite, and goethite.

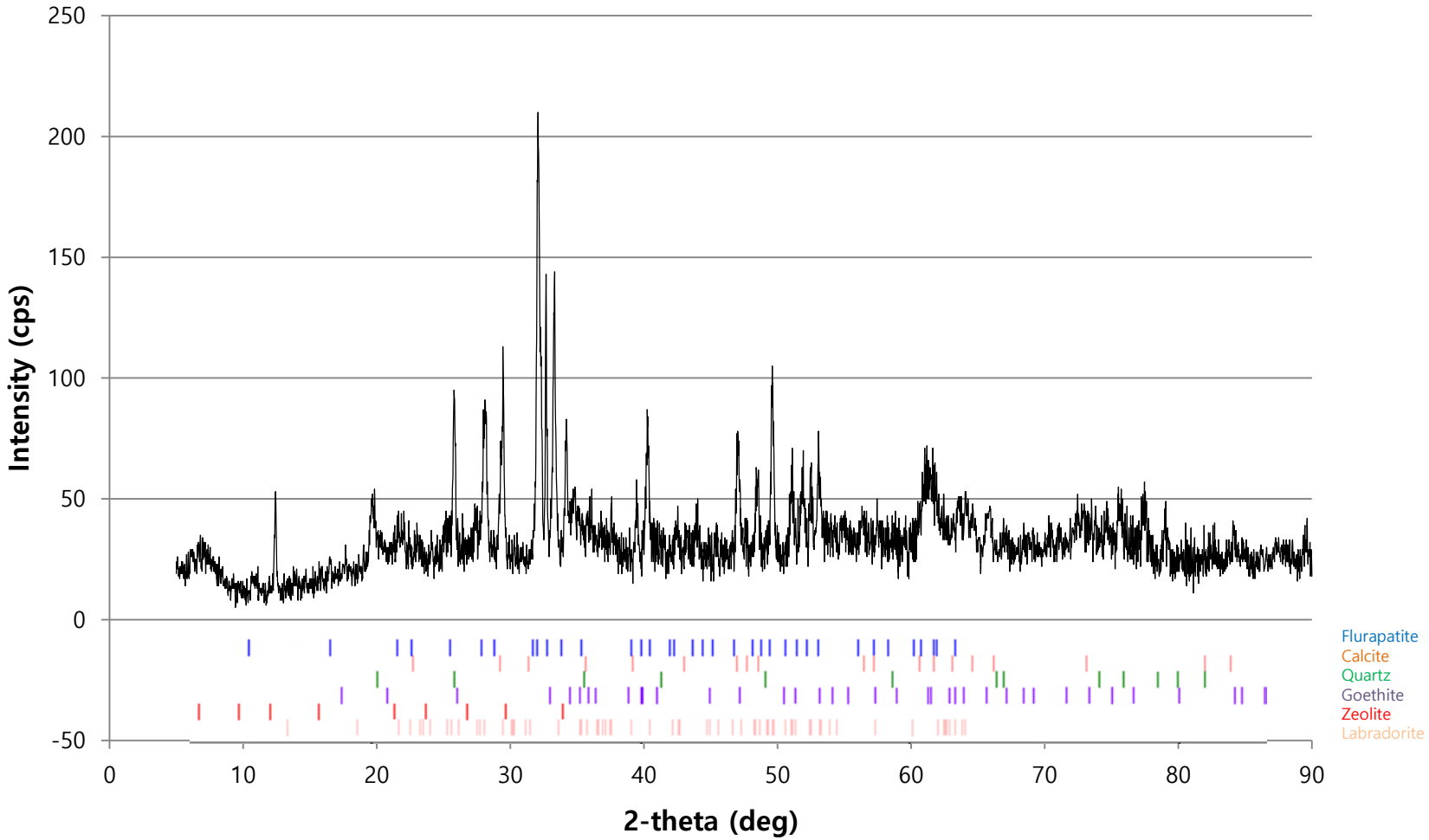

Figure 8. XRD result of phosphatized layer CD 5-5. Major peaks are coincident with fluorapatite, calcite, quartz, goethite, and labradorite.

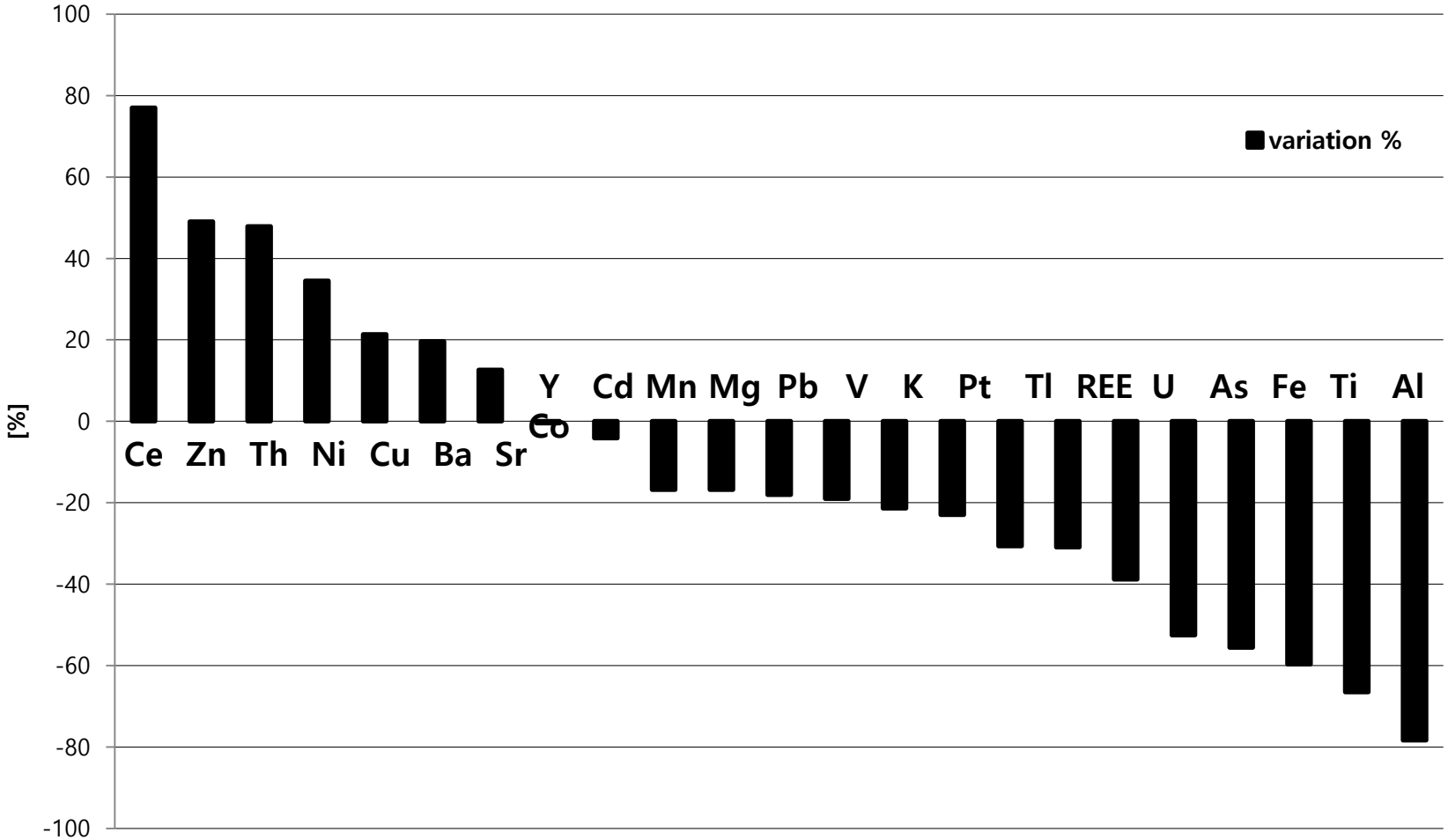

Figure 9. Variation between phosphatized crust and non-phosphatized crust of CD5-5. 0% is same with non-phosphatized crust concentration. REE represent lanthanides except Ce. P and Ca are excluded in this figure due to their high variation, 830% and 357% respectively.

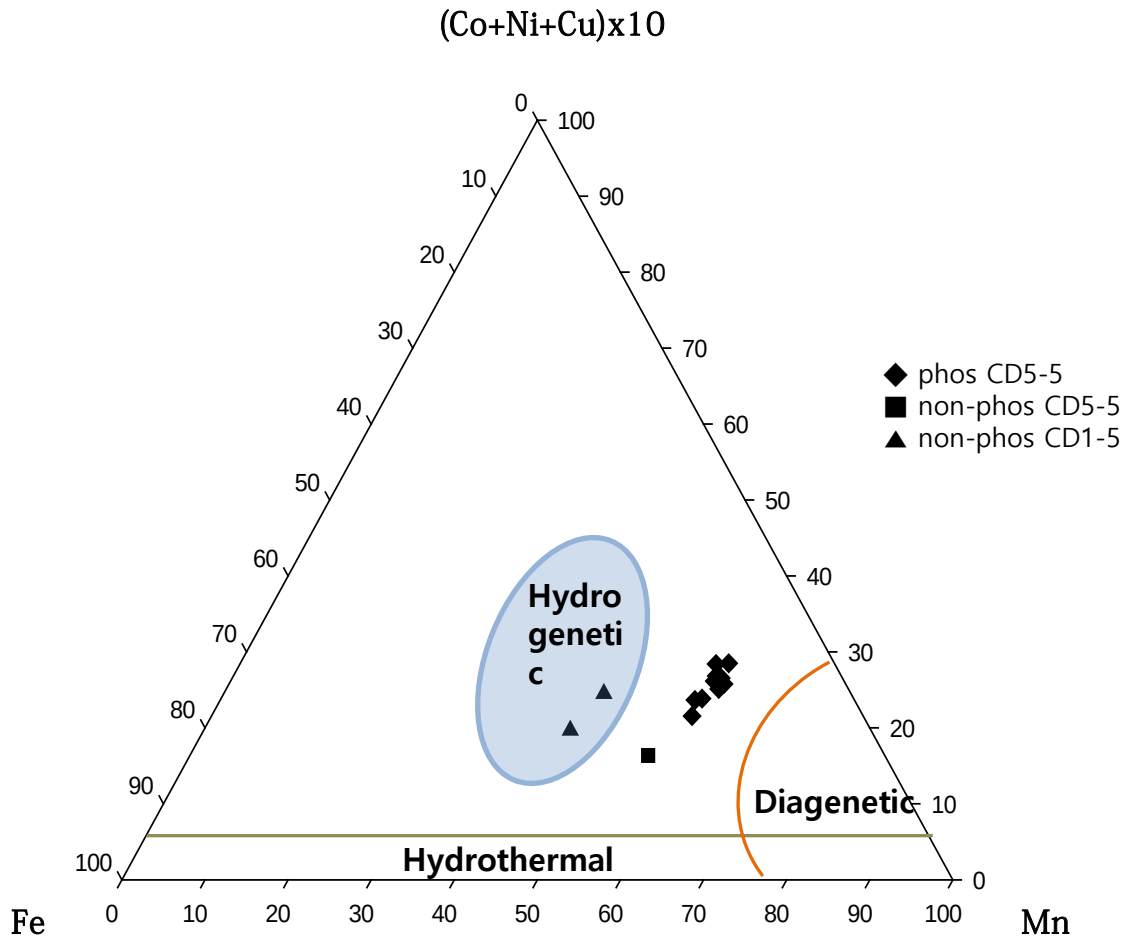

Figure 10. Classification of ferromanganese crusts from the Lemkein seamount using ternary diagram.

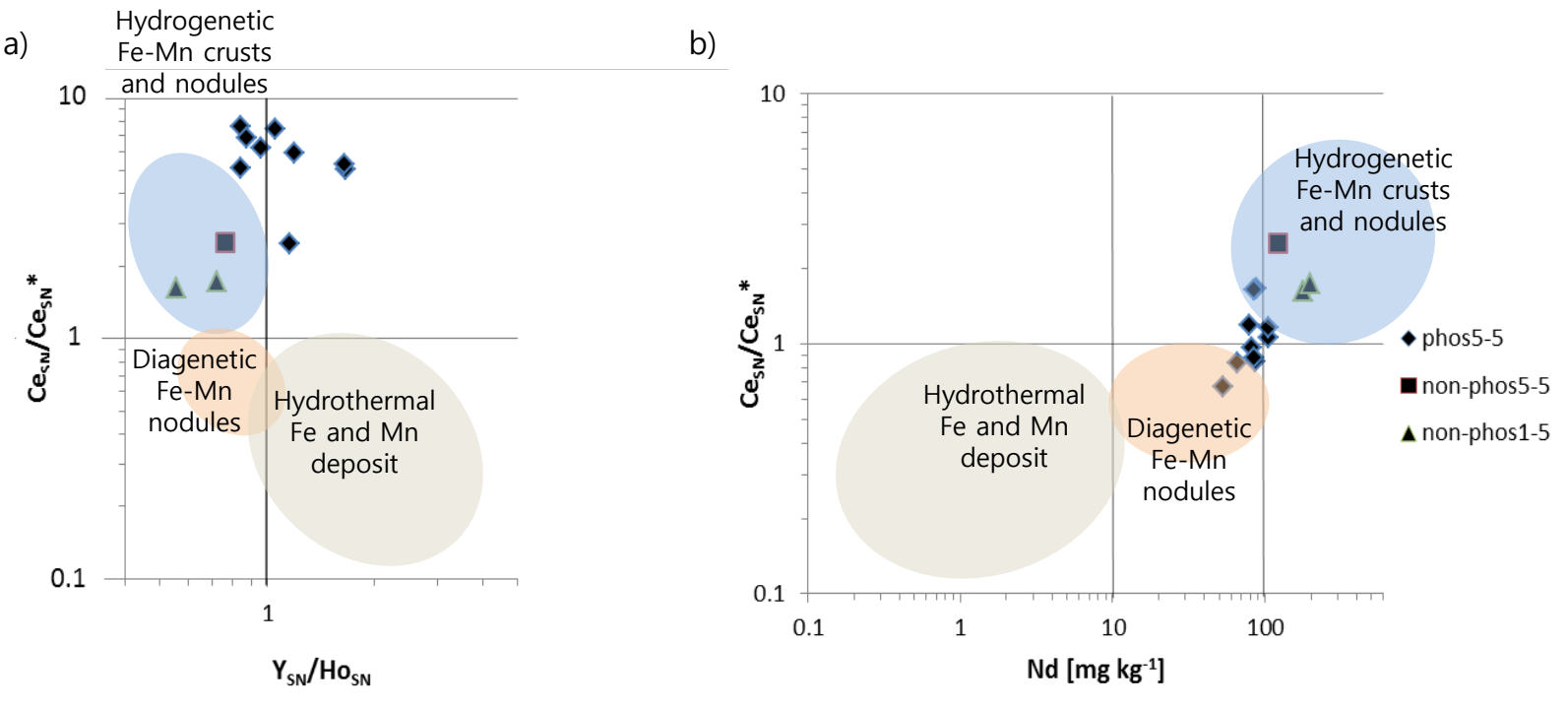

Figure 11. Classification of ferromanganese crusts from the Lemkein seamount based REY. a) Ce_{SN}/Ce_{SN}^* ratio vs Nd concentration and b) Ce_{SN}/Ce_{SN}^* ratio vs Y_{SN}/Ho_{SN} ratio. REY_{SN} indicates PAAS normalized value. Ce_{SN}^* is calculated as $Ce_{SN}^* = 0.5La_{SN} + 0.5Pr_{SN}$.

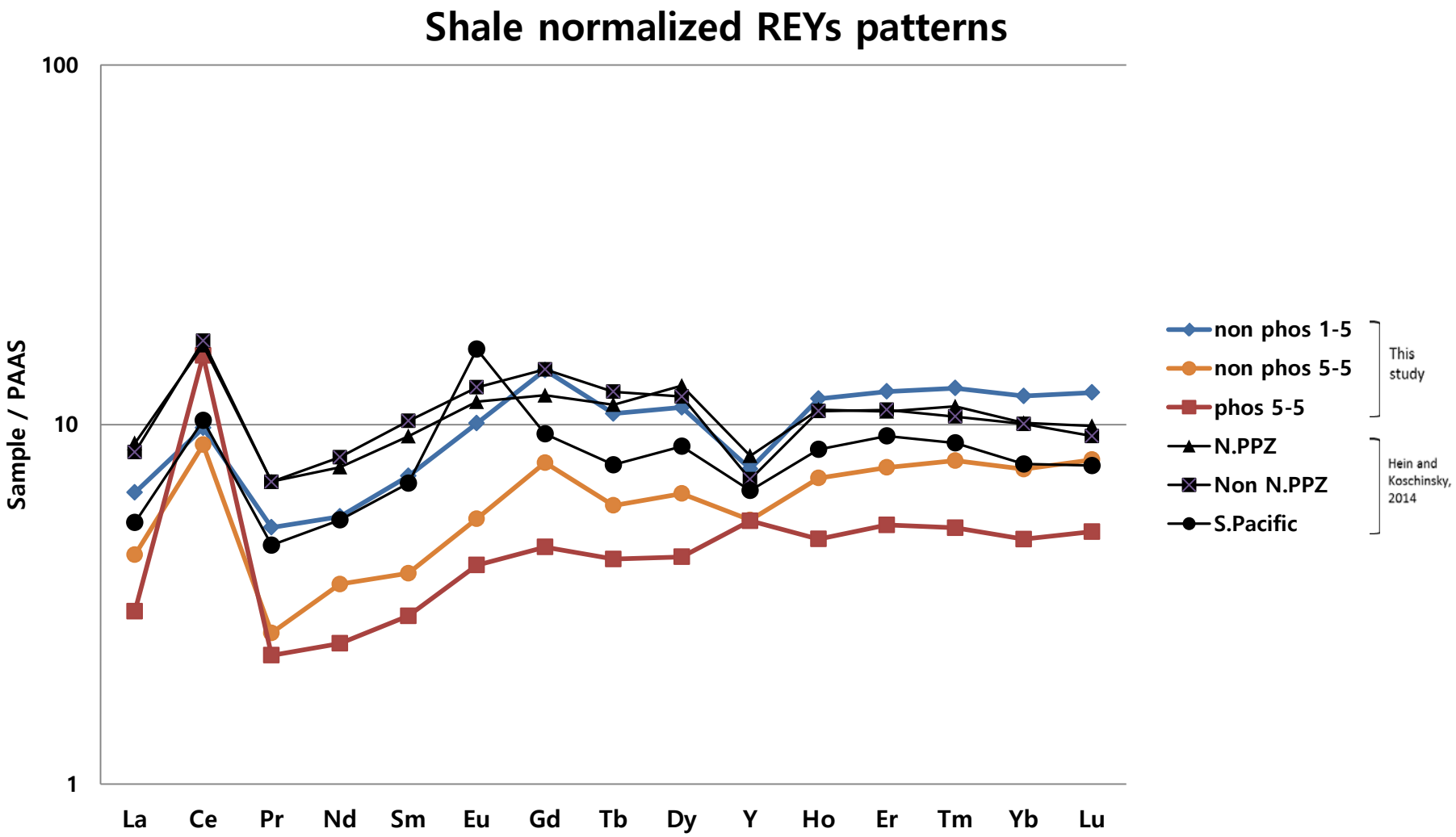

Figure 12. REY pattern of phosphatized crusts CD 5-5 from the Lemkein seamount.

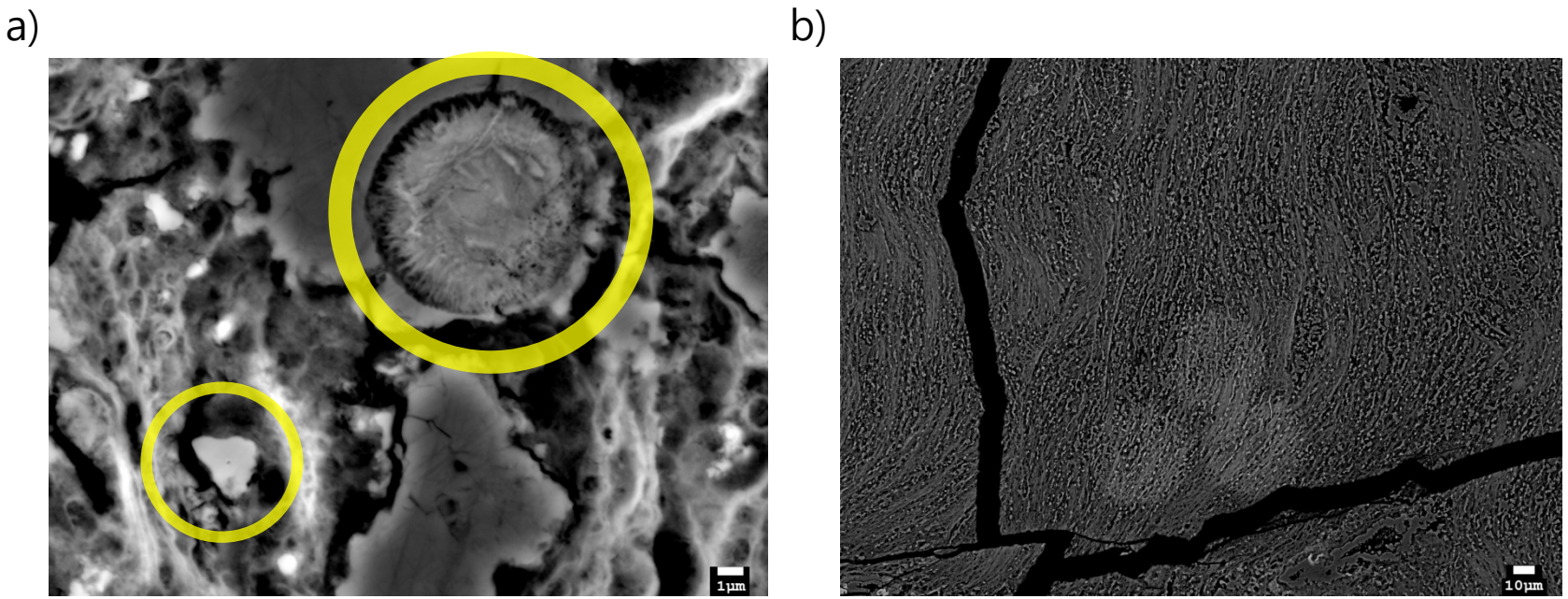

Figure 13. BSE images of phosphatized crust CD 5-5 after EPMA. a) Traces of EPMA on CFA. b) Traces of defocused beam on Fe-bearing vernadite phases.

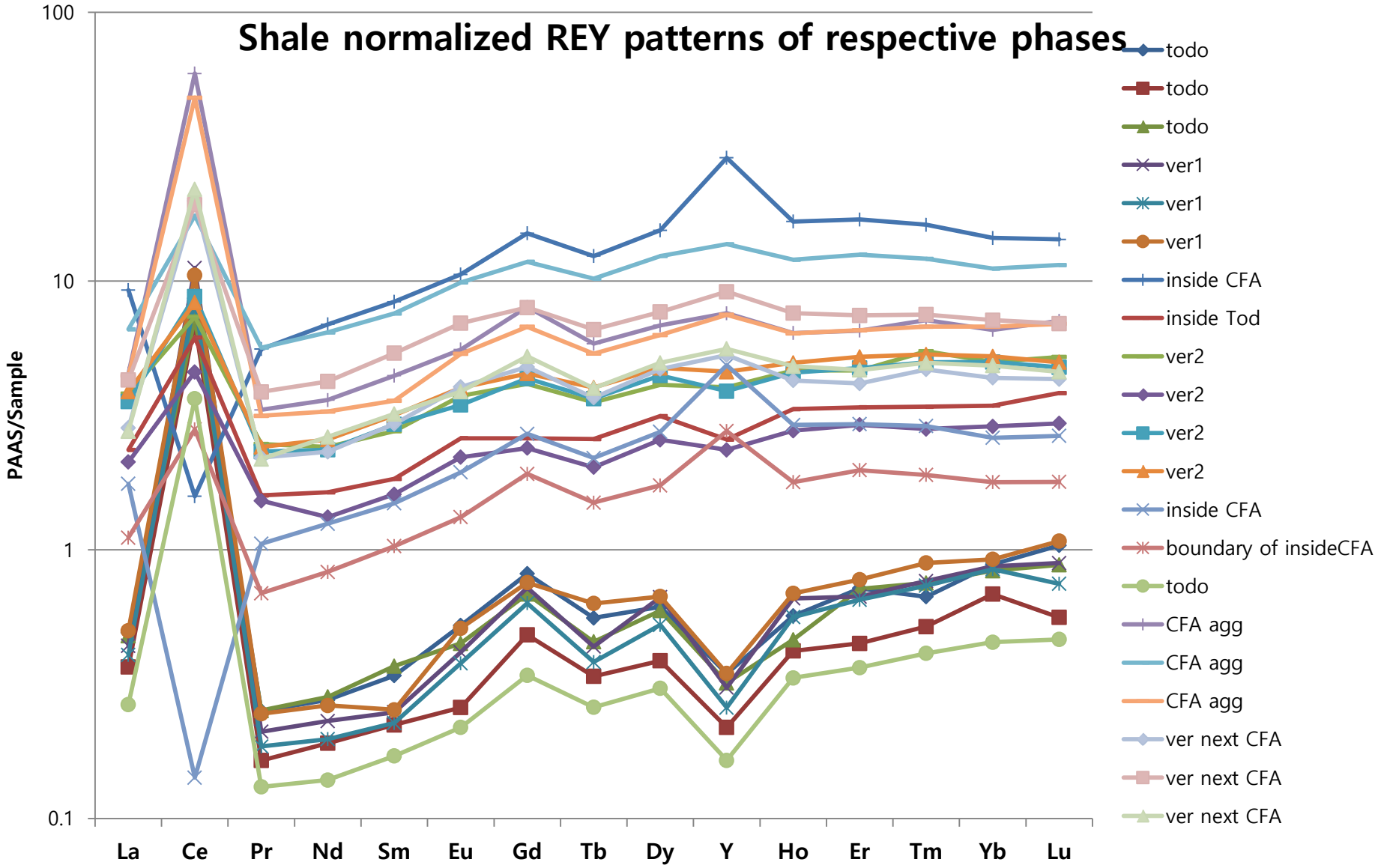

Figure 14. REY pattern of respective phases in phosphatized crusts CD 5-5 measured by LA-ICP-MS.

초록

서태평양 렘케인 해산의 인산염화 작용으로 인한 망간각의 원소 변화와 희토류 원소의 조절 요인

인산염화 작용이 망간각의 원소 조성에 끼치는 영향을 보기 위해 렘케인 해산의 인산염화 작용을 받은 망간각을 분석하였다. 주요 광물 상과 조성이 SEM과 XRD를 통해서 확인 하였다. CD 5-5의 인산염화 작용을 받은 층의 하부에서 10개의 샘플이 드릴링을 통해서 채취되었다. ICP-AES와 ICP-MS를 통해 주원소와 미량원소가 분석되었다. 채취된 부분의 맞은 편 면은 박편으로 만들어 EPMA와 LA-ICP-MS 분석을 하였다. Co, Al, Ti, Fe, As, Mn은 인산염화 작용을 받은 층에서 받지 않은 층에 비해 고갈된 반면, Zn, Ni, Cu는 부화되었다. 이러한 원소 차이의 경향성은 망간산화물의 재결정화와 철과 관련된 상들의 감소, 탄산염 플루오라파타이트의 형성과 연관이 있다. Ce의 농축이 REY 분류표를 통해 관찰되었고, Ce과 Mn의 강한 연관성이 나타났다. 이를 통해서 Ce이 탄산염 플루오라파타이트보다는 망간산화물에 농축됨을 알 수 있다. Ce과 REE의 연관성이 원자번호가 커짐에 따라 커지는 경향성이 관찰되었다. 이는 비슷한 P 함량을 가지는 인산염

화 작용을 받은 망간각에서는 탄산염 플루오라파타이트의 조성에 따라 REE 함량이 조절됨을 보여준다. Y도 같은 연관성을 보이나 REE보다 뚜렷하지는 않다. LA-ICP-MS 분석에서 서로 다른 광물 상의 REY 조성 차이가 뚜렷하게 나타났다. 총 REE 함량은 CFA에서 가장 부화되었고, 토도로카이트에서 가장 고갈되었다. 인산염화 작용을 받은 층에서의 망간각의 REY함량은 초기 상들의 손실과 인산염화 작용을 통한 보충의 결과로서 조절된다.

주요 용어 : 망간각, 희토류 원소와 이트륨 (REY), 인산염화 작용, 탄산염 플루오라파타이트 (CFA), Ca/P 비율

학 번 : 2013-20346